J. Fluid Mech. (2011), *vol.* 687, *pp.* 209–237.
doi:10.1017/jfm.2011.347

Rheology of a suspension of elastic particles in a viscous shear flow

Tong Gao, Howard H. Hu† and Pedro Ponte Castañeda

Department of Mechanical Engineering and Applied Mechanics, University of Pennsylvania, Philadelphia, PA 19104, USA

(Received 28 January 2011; revised 28 July 2011; accepted 11 August 2011; first published online 14 October 2011)

In this paper we consider a suspension of elastic solid particles in a viscous liquid. The particles are assumed to be neo-Hookean and can undergo finite elastic deformations. A polarization technique, originally developed for analogous problems in linear elasticity, is used to establish a theory for describing the finite-strain, time-dependent response of an ellipsoidal elastic particle in a viscous fluid flow under Stokes flow conditions. A set of coupled, nonlinear, first-order ODEs is obtained for the evolution of the uniform stress fields in the particle, as well as for the shape and orientation of the particle, which can in turn be used to characterize the rheology of a dilute suspension of elastic particles in a shear flow. When applied to a suspension of cylindrical particles with initially circular cross-section, the theory confirms the existence of steady-state solutions, which can be given simple analytical expressions. The two-dimensional, steady-state solutions for the particle shape and orientation, as well as for the effective viscosity and normal stress differences in the suspension, are in excellent agreement with direct numerical simulations of multiple-particle dispersions in a shear flow obtained by using an arbitrary Lagrangian–Eulerian (ALE) finite element method (FEM) solver. The corresponding solutions for the evolution of the microstructure and the rheological properties of suspensions of initially spherical (three-dimensional) particles in a simple shear flow are also obtained, and compared with the results of Roscoe (*J. Fluid Mech.*, vol. 28, 1967, pp. 273–293) in the steady-state regime. Interestingly, the results show that sufficiently soft elastic particles can be used to reduce the effective viscosity of the suspension (relative to that of the pure fluid).

Key words: particle/fluid flow, rheology, viscoelasticity

1. Introduction

The macroscopic rheological behaviour of colloidal suspensions has received considerable attention in the past. One interesting aspect of this problem is that colloidal systems in nature often contain micro-scaled soft and deformable inclusions that may affect the overall rheological properties of the solid–liquid mixture. A standard example is provided by the deformation, reorientation and aggregation of red blood cells, which are responsible for shear thinning and the viscoelastic response of human blood (Chien *et al.* 1967*a*,*b*). Colloidal suspensions with micro-scaled

† Email address for correspondence: hhu@seas.upenn.edu

soft objects (vesicles, droplets, etc.) are also commonly seen in a wide range of engineering applications, such as material synthesis and microfluidics (Barnes 1994; Subramaniam *et al.* 2005; Mattsson *et al.* 2009). Not surprisingly, the rheological behaviour of colloidal suspensions of deformable inclusions can be significantly different from suspensions of rigid inclusions (Einstein 1906). In general, the deformation of particles in a moving fluid depends on the applied hydrodynamic surface forces, the particle geometry and its material properties.

In the past decades, several authors have studied these systems both analytically and numerically. Fröhlich & Sack (1946) were the first to investigate a suspension of Hookean elastic spherical particles in a Newtonian fluid undergoing pure extensional motion. A linearized Oldroyd-type constitutive equation was derived to relate the macroscopic extensional stress and the strain rate. Oldroyd (1953) considered suspensions of Newtonian droplets in another Newtonian liquid with constant interfacial tension. It was found that due to the surface tension and deformation of the droplets, the suspension exhibits viscoelastic behaviour with an Oldroyd-type constitutive relation. In fact, the rheological behaviour of such suspensions is similar to that of a suspension of elastic particles in a Newtonian fluid. In a separate development, Cerf (1952) investigated a suspension of spheres with special viscoelastic properties in a viscous liquid under oscillatory motion of small amplitude. Generalizing Cerf's work for finite deformations, Roscoe (1967) investigated the rheological behaviour of a suspension of viscoelastic spheres in a viscous liquid. In Roscoe's work, it was shown that steady-state solutions are possible for initially spherical particles, such that the particle deforms into an ellipsoid of fixed orientation, and the material within the ellipsoid deforms continuously and rotates with steady homogeneous (i.e. constant) velocity gradient and stress. The effective viscosity and normal stress differences for the suspension were derived as functions of the solid and liquid material properties and the flow conditions. At about the same time, Goddard & Miller (1967) independently investigated the time-dependent version of the problem with viscoelastic particles in a Newtonian liquid, but restricting the analysis to small deformations in the particles. By making use of Jeffery's solution (Jeffery 1922) for flow around rigid particles, the authors solved for the homogeneous deformation of the particle. Based on the coupled solutions for the flow field around the particle and the deformation of the particle, they derived the constitutive equations for the rheological behaviour of the suspension of slightly deformed spheres in the dilute limit. It was pointed out that the ellipticity of the deformed spheres contributed to nonlinear terms in the macroscopic constitutive equation for the suspension. Other related works in this area, mentioned only briefly here, include the following. In the small deformation limit, Murata (1981) studied deformation of an spherical elastic particle in an arbitrary flow field by using a perturbation analysis. Snabre & Mills (1999) proposed a self-consistent model with an effective medium approximation for estimating the effective shear viscosity of a non-dilute suspension of viscoelastic particles. In addition, numerous works have been published on suspensions of cells/vesicles (Taylor 1934; Rumscheidt & Mason 1961; Barthès-Biesel 1980; Barthès-Biesel & Rallison 1981; Keller & Skalak 1982; Ramanujan & Pozrikidis 1998; Lac *et al.* 2004; Ghigliotti, Biben & Misbah 2010).

The objective of the present work is to explore the rheological properties of suspensions of nonlinearly elastic particles in the regime of arbitrarily large deformations. The shear flow problem for a suspension of neo-Hookean, elastic particles in a Newtonian viscous fluid is revisited analytically and numerically. For this purpose, we rewrite the constitutive equation for the neo-Hookean material as

an evolution equation for the stress tensor, which involves the velocity gradient of the deformation. This constitutive equation is materially frame-indifferent and does not involve the displacement field. Fully coupled, fluid–solid simulations at small Reynolds number for an isolated inclusion suggest that the strain rate and elastic stress are uniformly distributed inside the solid particle. Motivated by this observation, in this work, we make use a polarization technique derived from the classical work of Eshelby (1957, 1959) in the theory of composite materials to derive an exact analytical solution for the isolated particle problem under Stokes flow conditions. The solution for this problem is then used in a consistent fashion to evaluate the macroscopic rheological behaviour of the suspension in the dilute limit. The analytical results for dilute concentrations are compared with full numerical simulations for small concentrations of particles in an effort to estimate the domain of validity of the dilute theory.

The numerical technique used here is a monolithic finite element method (FEM) solver developed by Gao & Hu (2009), based on the arbitrary Lagrangian–Eulerian (ALE) method (Hirt, Amsden & Cook 1974; Hu, Zhu & Patankar 2001). The unique advantage of our solver is that the unknown variables in both the fluid and solid phases are the velocity, pressure and stress. The displacement field is not involved in the formulation. Consistent time-integration schemes and discretizing methods are employed for all physical variables, leading to a nonlinear system which can be solved by efficient iterative schemes with appropriate preconditioners. Thus we can solve the coupled equations for the fluid and solid phases simultaneously. For the two-dimensional case, we simulate the suspension by considering multiple particles in a shear flow confined between two parallel plates.

The paper is organized as follows. § 2 is dedicated to the mathematical formulation of the problem. In § 3, a polarization technique based on Eshelby's solution is introduced and used to show that the velocity gradient is uniform inside the isolated elastic particle provided that its shape is instantaneously ellipsoidal. In § 4, the results of § 3 are used to obtain a set of coupled, nonlinear ODEs characterizing the evolution of the particle shape and orientation, as well as the stresses inside the particle for the general case of an initially ellipsoidal particle and uniform remote flow conditions. The rheological properties are then calculated accordingly in the dilute limit. In § 5, the theory is first applied to the idealized two-dimensional problem consisting of transverse shear flow of a dispersion of aligned cylindrical particles with initially circular cross-section, and a closed-form analytical solution is obtained for steady-state conditions. The effective behaviour of the suspension in the dilute limit is then derived using the single particle solutions. The analytical solution for dilute concentrations is compared with the results of a direct numerical simulation for multiple elastic particles in a shear flow. In § 6, initially spherical (three-dimensional) particles are considered, and the steady-state solutions are compared with the results by Roscoe (1967). In addition, the time evolution of the rheological properties of the suspension of such three-dimensional particles is computed and analysed. Finally, some conclusions are drawn in § 7.

2. Mathematical formulation

Consider a suspension of neo-Hookean elastic particles in a Newtonian liquid. The particles are distributed in such a way that the resulting solid–liquid mixture is heterogeneous but statistically uniform. In the fluid domain (Ω_f), the fluid flow is

governed by the incompressible Navier–Stokes equations,

$$\nabla \cdot \boldsymbol{v}_f = 0, \tag{2.1}$$

$$\rho_f \left[\frac{\partial \boldsymbol{v}_f}{\partial t} + \left(\boldsymbol{v}_f \cdot \nabla \right) \boldsymbol{v}_f \right] = \nabla \cdot \boldsymbol{\sigma}_f, \tag{2.2}$$

where ρ_f is the fluid density, $\boldsymbol{v}_f$ is the fluid velocity, and $\boldsymbol{\sigma}_f$ is the stress in the Newtonian fluid defined by the constitutive relation:

$$\boldsymbol{\sigma}_f = -p_f \boldsymbol{I} + \boldsymbol{\tau}_f = -p_f \boldsymbol{I} + 2\mu_f \boldsymbol{D}_f, \tag{2.3}$$

where μ_f is the viscosity, p_f is the pressure, $\boldsymbol{\tau}_f$ is the extra stress tensor, and $\boldsymbol{D}_f = (1/2)[\nabla \boldsymbol{v}_f + (\nabla \boldsymbol{v}_f)^{\mathrm{T}}]$ is the rate-of-deformation or strain rate tensor in the fluid phase.

In the particles (Ω_p), the solid phase is also assumed to be incompressible. The conservation of mass and momentum then also require that

$$\nabla \cdot \boldsymbol{v}_s = 0, \tag{2.4}$$

$$\rho_s \left[\frac{\partial \boldsymbol{v}_s}{\partial t} + (\boldsymbol{v}_s \cdot \nabla) \boldsymbol{v}_s \right] = \nabla \cdot \boldsymbol{\sigma}_s, \tag{2.5}$$

where ρ_s is the solid density, $\boldsymbol{v}_s$ is the solid velocity, and $\boldsymbol{\sigma}_s$ is the total stress tensor in the solid phase. For an incompressible, neo-Hookean solid, the constitutive relation between stress and strain can be written as (Macosko 1994; Ogden 1984)

$$\boldsymbol{\sigma}_s = -p_s \boldsymbol{I} + \boldsymbol{\tau}_s = -p_s \boldsymbol{I} + \eta_s (\boldsymbol{B}_s - \boldsymbol{I}), \tag{2.6}$$

where η_s is the shear modulus, $\boldsymbol{I}$ is the identity tensor, $\boldsymbol{B}_s = \boldsymbol{F}_s \boldsymbol{F}_s^{\mathrm{T}}$ is the Finger (or left Cauchy–Green) tensor, with $\boldsymbol{F}_s = \partial \boldsymbol{x} / \partial \boldsymbol{X}$ denoting the deformation gradient tensor in the solid phase. In addition, $\boldsymbol{\tau}_s = \eta_s (\boldsymbol{B}_s - \boldsymbol{I})$ is the 'extra stress' tensor which is not 'deviatoric' since in general $\mathrm{tr}(\boldsymbol{\tau}_s) \neq 0$. Likewise, p_s is a pseudo-pressure, which has no physical significance, serving only as a Lagrangian multiplier to enforce the incompressibility constraint in the solid. More detailed discussions on the definition of the pressure and extra stress for anisotropic stress fields can be found in early works on elasticity (Rivlin 1948). Using the well-known identity $(\mathrm{D}\boldsymbol{F}_s/\mathrm{D}t) = (\nabla \boldsymbol{v}_s)\boldsymbol{F}_s$, it is straightforward to show that the rate of change of the Finger tensor (in the solid) satisfies (Joseph 1990)

$$\frac{\mathrm{D}\boldsymbol{B}_s}{\mathrm{D}t} = (\nabla \boldsymbol{v}_s)\boldsymbol{B}_s + \boldsymbol{B}_s (\nabla \boldsymbol{v}_s)^{\mathrm{T}}. \tag{2.7}$$

Then, making use of (2.6), the following evolution equation is obtained for the extra stress tensor:

$$\overset{\nabla}{\boldsymbol{\tau}}_s = \frac{\mathrm{D}\boldsymbol{\tau}_s}{\mathrm{D}t} - (\nabla \boldsymbol{v}_s)\boldsymbol{\tau}_s - \boldsymbol{\tau}_s (\nabla \boldsymbol{v}_s)^{\mathrm{T}} = \eta_s [\nabla \boldsymbol{v}_s + (\nabla \boldsymbol{v}_s)^{\mathrm{T}}], \tag{2.8}$$

where $\overset{\nabla}{\boldsymbol{\tau}}_s$ is the (so-called) upper-convected time derivative, and where $\mathrm{D}\boldsymbol{\tau}_s/\mathrm{D}t = (\partial \boldsymbol{\tau}_s/\partial t) + \boldsymbol{v}_s \cdot \nabla \boldsymbol{\tau}_s$ denotes the material time derivative of the extra stress. Equation (2.8) can be viewed as a special case of the constitutive equation for an upper-convected Maxwell fluid when its relaxation time tends to infinity, and the ratio of the fluid viscosity and the relaxation time tends to the shear modulus η_s.

The governing equations may be put in dimensionless form by choosing the characteristic velocity scale $\dot{\gamma} d_p$, the length scale d_p, the time scale $\dot{\gamma}^{-1}$, the pressure and stress scale $\mu_f \dot{\gamma}$, where d_p is the particle diameter and $\dot{\gamma}$ is the applied shear

rate in the bulk fluid. Here, for simplicity, we use the same notation for the dimensionless variables as for their dimensional counterparts. The dimensionless forms of the governing equations ((2.2), (2.3), (2.5) and (2.8)) thus become

$$Re\left(\frac{\partial \boldsymbol{v}_f}{\partial t}+\boldsymbol{v}_f\cdot\nabla\boldsymbol{v}_f\right)=-\nabla p_f+\nabla\cdot\boldsymbol{\tau}_f, \tag{2.9}$$

$$\boldsymbol{\tau}_f=\nabla\boldsymbol{v}_f+(\nabla\boldsymbol{v}_f)^{\mathrm{T}}, \tag{2.10}$$

$$Re\left(\frac{\partial \boldsymbol{v}_s}{\partial t}+\boldsymbol{v}_s\cdot\nabla\boldsymbol{v}_s\right)=-\nabla p_s+\nabla\cdot\boldsymbol{\tau}_s, \tag{2.11}$$

$$G\left[\frac{\partial \boldsymbol{\tau}_s}{\partial t}+\boldsymbol{v}_s\cdot\nabla\boldsymbol{\tau}_s-(\nabla\boldsymbol{v}_s)\,\boldsymbol{\tau}_s-\boldsymbol{\tau}_s(\nabla\boldsymbol{v}_s)^{\mathrm{T}}\right]=\nabla\boldsymbol{v}_s+(\nabla\boldsymbol{v}_s)^{\mathrm{T}}, \tag{2.12}$$

where $Re=\rho\dot{\gamma}d_p^2/\mu_f$ is the Reynolds number, and

$$G=\frac{\mu_f\dot{\gamma}}{\eta_s} \tag{2.13}$$

is a dimensionless parameter representing the ratio of the viscous forces in the fluid to the elastic forces in the solid. (Note that G is related to the Deborah number in macroscopic rheology.) Therefore, the bigger the G number is, the larger is the elastic deformation in the particles. In the above non-dimensionalization, we have assumed the particles are neutrally buoyant ($\rho_f=\rho_s=\rho$). Furthermore, in this study, we will only consider the Stokes flow regime, $Re\to 0$, so the left-hand sides of equations (2.9) and (2.11) can be neglected.

Finally, at the fluid–solid interface, the velocity should satisfy the no-slip condition

$$\boldsymbol{v}_f=\boldsymbol{v}_s, \tag{2.14}$$

while the traction $\boldsymbol{\sigma}\cdot\boldsymbol{n}$ is required to be continuous across the interface

$$\boldsymbol{\sigma}_f\cdot\boldsymbol{n}=\boldsymbol{\sigma}_s\cdot\boldsymbol{n}, \tag{2.15}$$

where $\boldsymbol{n}$ is the unit outward normal vector at the interface.

In summary, the system of (2.9)–(2.12), which was obtained by Gao & Hu (2009), together with the incompressibility constraints in the fluid and solid (2.1) and (2.4), and the continuity conditions (2.14) and (2.15), as well as appropriate far-field boundary conditions, serve to determine the velocity and stress field everywhere in the particles and the embedding fluid. This approach avoids the need to solve for the displacement and strain fields in the particles associated with more conventional approaches, which are known to lead to convergence problems (Masud & Hughes 1997; Le Tallec & Mouro 2001).

In general, to determine the overall behaviour of the suspension, it is necessary to carefully select a representative volume element (RVE) of the bulk specimen. The effective fields are derived by suitable averaging of the microscopic fields over the RVE (Batchelor 1970; Willis 1981). When the concentration is low, and all the inclusions are well separated by large inter-particle distances, the particle–particle interactions may be neglected. Thus, in the dilute limit, the effective field is solely determined by the behaviour of a single particle in an unbounded fluid, and it becomes necessary to first understand the response of a single particle deforming in an unbounded shear flow. In the next section, we consider the instantaneous response of the single particle problem.

3. The instantaneous response of an ellipsoidal, elastic inclusion

It is known from the works of Roscoe (1967) and Goddard & Miller (1967) that an initially spherical particle with viscoelastic constitutive behaviour in an unbounded Newtonian fluid admits under certain conditions a steady-state solution where the particle becomes ellipsoidal with constant stress, strain rate and vorticity. Moreover, as is well known (Bilby, Eshelby & Kundu 1975; Bilby & Kolbuszewski 1977; Ogden 1984; Wetzel & Tucker 2001), uniform (but possibly time-dependent) strain rate and vorticity fields in the particle would imply that the particle moves through a sequence of ellipsoidal shapes until the final steady-state shape (if such a steady state exists) where the strain rate and vorticity fields no longer change. Inspired by these findings, in this section, we seek to demonstrate that the solution for an isolated, elastic, ellipsoidal particle in an unbounded Newtonian viscous fluid is indeed such that the strain rate and vorticity fields are uniform inside the particle. Because of the well-known mathematical analogy between linear elasticity and Stokes flow, the classical solution of Eshelby (1957, 1959) for the response of an isolated, linear-elastic, ellipsoidal inclusion in an infinite matrix of a different linear elastic medium have been adapted for the problem of Newtonian droplets (Bilby *et al.* 1975; Bilby & Kolbuszewski 1977; Wetzel & Tucker 2001). In addition, variational approximations have been given by Kailasam & Ponte Castañeda (1998) for non-dilute concentrations of particles and nonlinearly viscous behaviour for the matrix and inclusion phases, building on the Hashin–Shtrikman-type estimates of Ponte Castañeda & Willis (1995) for 'ellipsoidal' distributions of elastic particles in a linear elastic matrix. In this work, we will make use of the polarization technique developed by Willis (1981) for the single inclusion problem in a general anisotropic elastic matrix. This technique consists in rewriting the boundary value problem for the inclusion in an unbounded medium in terms of an integral equation for the polarization inside the inclusion. Using this formulation, it is straightforward to show that the exact solution for the polarization (and, therefore, for the associated strain and stress fields) is constant inside the inclusion, provided that the shape of the inclusion is ellipsoidal. For completeness, the application of this technique to the problem of interest here is described in some detail next.

Thus, in this section, we consider the problem of an isotropic, incompressible, elastic inclusion with an instantaneously ellipsoidal shape in a Newtonian fluid of infinite extent. In the limit of vanishingly small Reynolds number ($Re \to 0$), the continuity and momentum equations ((2.1), (2.4), (2.9) and (2.11)) can be simply written as

$$\nabla \cdot \boldsymbol{v} = 0, \quad \text{and} \quad \nabla \cdot \boldsymbol{\sigma} = 0, \tag{3.1}$$

for all of space, including both the solid and fluid phases. Next, we introduce a uniform, incompressible 'reference' medium with the same viscosity μ_f as the fluid phase, and define the dimensionless stress polarization tensor $\boldsymbol{\Xi}$ as the difference between the total stress in the actual suspension $\boldsymbol{\sigma}$ and the stress in an incompressible, homogeneous, reference medium, as given by $-p\boldsymbol{I}+2\boldsymbol{D}$, where $\boldsymbol{D} = (1/2)[\nabla\boldsymbol{v}+(\nabla\boldsymbol{v})^{\mathrm{T}}]$ is the strain rate tensor, and p is the hydrostatic pressure. It is then possible to define a non-dimensionalized polarization tensor

$$\boldsymbol{\Xi} = \boldsymbol{\sigma} + p\boldsymbol{I} - 2\boldsymbol{D}, \tag{3.2}$$

which is obviously non-zero ($\boldsymbol{\Xi} \neq \mathbf{0}$) only inside the elastic particle, denoted Ω_p. Thus, (3.1) can be written in the form

$$\nabla \cdot \boldsymbol{v} = 0, \quad \nabla^2 \boldsymbol{v} - \nabla p + \nabla \cdot \boldsymbol{\Xi} = 0, \tag{3.3}$$

which can be reinterpreted as a new problem for the homogeneous reference medium subjected to a distribution of body force, given by $\nabla \cdot \boldsymbol{\Xi}$ in Ω_p. In addition, we enforce the asymptotic Dirichlet-type boundary condition on the velocity:

$$\boldsymbol{v} = \boldsymbol{L}^0 \boldsymbol{x} \text{ as } |\boldsymbol{x}| \to \infty, \tag{3.4}$$

which is consistent with a uniform (prescribed) velocity gradient tensor $\boldsymbol{L}^0$.

Because of the linearity of the boundary value problem defined by (3.3) and (3.4), the velocity field may be written in the form

$$v_i(\boldsymbol{x}) = L^0_{ij} x_j + \int_{\Re^3} G_{ip}(\boldsymbol{x}, \boldsymbol{x}') \frac{\partial \Xi_{pq}}{\partial x'_q}(\boldsymbol{x}') \, \mathrm{d}\boldsymbol{x}', \tag{3.5}$$

where

$$G_{ip}(\boldsymbol{x}, \boldsymbol{x}') = \frac{1}{8\pi |\boldsymbol{x} - \boldsymbol{x}'|} \left(\frac{(x_i - x'_i)(x_p - x'_p)}{|\boldsymbol{x} - \boldsymbol{x}'|^2} + \delta_{ip} \right) \tag{3.6}$$

is the infinite-body Green's function associated with the differential operators in (3.3) and (3.4), also known as the Oseen tensor, or Stokeslet. (It should be noted that the pressure p is given by a corresponding expression in terms of the polarization $\boldsymbol{\Xi}$, but it will not be needed in the developments to follow and therefore will not be displayed here.) Integrating expression (3.5) by parts, using the facts that the Green's function vanishes when $r = |\boldsymbol{x} - \boldsymbol{x}'| \to \infty$ and $(\partial G_{ip}/\partial x'_q)(\boldsymbol{x}, \boldsymbol{x}') = -(\partial G_{ip}/\partial x_q)(\boldsymbol{x}, \boldsymbol{x}')$, and that $\boldsymbol{\Xi}$ is non-zero only inside the particle (Ω_p), we have

$$v_i(\boldsymbol{x}) = L^0_{ij} x_j + \frac{\partial}{\partial x_q} \int_{\Omega_p} G_{ip}(\boldsymbol{x}, \boldsymbol{x}') \Xi_{pq}(\boldsymbol{x}') \, \mathrm{d}\boldsymbol{x}'. \tag{3.7}$$

To avoid the difficulty with the singularity of the Oseen tensor $\boldsymbol{G}$ in expression (3.7), it is useful to make use of its Fourier space representation

$$\boldsymbol{G}(\boldsymbol{x}, \boldsymbol{x}') = \frac{1}{8\pi^3} \int_{\Re^3} \frac{1}{k^2} \left(\boldsymbol{I} - \frac{\boldsymbol{k} \otimes \boldsymbol{k}}{k^2} \right) \mathrm{e}^{\mathrm{i}\boldsymbol{k} \cdot (\boldsymbol{x} - \boldsymbol{x}')} \, \mathrm{d}\boldsymbol{k}, \tag{3.8}$$

where $k = |\boldsymbol{k}|$. Then, rewriting the integral in (3.8) in spherical coordinates, and performing the integration in the radial direction by means of the identity $\int_{-\infty}^{+\infty} \mathrm{e}^{\mathrm{i}\boldsymbol{k} \cdot (\boldsymbol{x} - \boldsymbol{x}')} \, \mathrm{d}k = 2\pi\delta(\boldsymbol{\xi} \cdot (\boldsymbol{x} - \boldsymbol{x}'))$, where $\boldsymbol{\xi} = \boldsymbol{k}/k$ is a unit vector and δ is the Dirac delta function, it follows that $\boldsymbol{G}$ can be written in the alternative form

$$\boldsymbol{G}(\boldsymbol{x}, \boldsymbol{x}') = \frac{1}{8\pi^2} \int_{|\boldsymbol{\xi}|=1} \boldsymbol{F}(\boldsymbol{\xi}) \delta(\boldsymbol{\xi} \cdot (\boldsymbol{x} - \boldsymbol{x}')) \, \mathrm{d}S, \tag{3.9}$$

where $\boldsymbol{F}(\boldsymbol{\xi}) = \boldsymbol{I} - \boldsymbol{\xi} \otimes \boldsymbol{\xi}$. It is emphasized that the integration over $\boldsymbol{\xi}$ in (3.9) is performed on the surface of the unit sphere. Expression (3.9) is a special case of a representation first obtained by Willis (1981) – by means of a plane-wave decomposition (Gel'fand & Shilov 1964) – for the corresponding Green's function in linear elasticity involving a generally anisotropic medium.

Thus, using expression (3.9) in (3.7) and interchanging the integrals over $\mathrm{d}S$ and $\mathrm{d}\boldsymbol{x}'$, it follows that

$$v_i(\boldsymbol{x}) = L^0_{ij}x_j + \frac{1}{8\pi^2}\int_{|\boldsymbol{\xi}|=1} \xi_q F_{ip}(\boldsymbol{\xi}) \int_{\Omega_p} \delta'(\boldsymbol{\xi}\cdot(\boldsymbol{x}-\boldsymbol{x}'))\,\Xi_{pq}(\boldsymbol{x}')\,\mathrm{d}\boldsymbol{x}'\,\mathrm{d}S, \tag{3.10}$$

where the derivative of δ is with respect to its scalar argument. The corresponding expressions for the strain rate $\boldsymbol{D}$ and vorticity tensor $\boldsymbol{W}$ $(=(1/2)(\nabla\boldsymbol{v}-(\nabla\boldsymbol{v})^{\mathrm{T}}))$ are then given by

$$D_{ij}(\boldsymbol{x}) = D^0_{ij} + \frac{1}{8\pi^2}\int_{|\boldsymbol{\xi}|=1} H_{ijpq}(\boldsymbol{\xi}) \int_{\boldsymbol{x}'\in\Omega_p} \delta''(\boldsymbol{\xi}\cdot(\boldsymbol{x}-\boldsymbol{x}'))\,\Xi_{pq}(\boldsymbol{x}')\,\mathrm{d}\boldsymbol{x}'\,\mathrm{d}S, \tag{3.11}$$

$$W_{ij}(\boldsymbol{x}) = W^0_{ij} + \frac{1}{8\pi^2}\int_{|\boldsymbol{\xi}|=1} T_{ijpq}(\boldsymbol{\xi}) \int_{\boldsymbol{x}'\in\Omega_p} \delta''(\boldsymbol{\xi}\cdot(\boldsymbol{x}-\boldsymbol{x}'))\,\Xi_{pq}(\boldsymbol{x}')\,\mathrm{d}\boldsymbol{x}'\,\mathrm{d}S, \tag{3.12}$$

where $\boldsymbol{D}^0$ $(\mathrm{tr}\,\boldsymbol{D}^0=0)$ and $\boldsymbol{W}^0$ are the (uniform) strain rate and vorticity tensors associated with the prescribed far-field velocity gradient $\boldsymbol{L}^0$. In these expressions, the fourth-order tensors $\mathbb{H}$ are $\mathbb{T}$ are defined by

$$H_{ijpq}(\boldsymbol{\xi}) = F_{ip}\xi_j\xi_q|_{(ij)(pq)}, \quad T_{ijpq}(\boldsymbol{\xi}) = F_{ip}\xi_j\xi_q|_{[ij](pq)}, \tag{3.13}$$

where the indices in parentheses, such as (ij), are to be symmetrized, while the indices in square brackets, such as $[ij]$, are to be anti-symmetrized.

Now, since the particle is ellipsoidal, the volume that it occupies may be written as $\Omega_p = \{\boldsymbol{x}, |\boldsymbol{Z}^{-T}\boldsymbol{x}| \leqslant 1\}$, where $\boldsymbol{Z}$ is the so-called shape tensor. In the principal coordinates defined by the axes of the (three-dimensional) ellipsoidal particle, $\boldsymbol{Z} = \mathrm{diag}\{a,b,c\}$ is a diagonal matrix with a,b,c being the three semi-axes of the ellipsoid. Then, introducing the new variables

$$\boldsymbol{y} = \boldsymbol{Z}^{-T}\boldsymbol{x}, \quad \boldsymbol{\eta} = \boldsymbol{Z}\boldsymbol{\xi}, \tag{3.14}$$

it can be shown (Willis 1981) that for any position vector $\boldsymbol{x}\in\Omega_p$ (or $|\boldsymbol{y}|\leqslant 1$), the integral

$$\int_{\boldsymbol{x}'\in\Omega_p} \delta''(\boldsymbol{\xi}\cdot(\boldsymbol{x}-\boldsymbol{x}'))\,\mathrm{d}\boldsymbol{x}' = \int_{|\boldsymbol{y}'|\leqslant 1} \delta''(\boldsymbol{\eta}\cdot(\boldsymbol{y}-\boldsymbol{y}'))\,\mathrm{d}\boldsymbol{y}' = -2\pi|\boldsymbol{\eta}|^{-3} \tag{3.15}$$

is independent of $\boldsymbol{x}$. It follows from this result, together with the fact that the strain rate in the particle is given by $\boldsymbol{D} = (\boldsymbol{\sigma}+p\boldsymbol{I}-\boldsymbol{\Xi})/2 = (\boldsymbol{\tau}-\boldsymbol{\Xi})/2$, that a uniform solution in (3.11) is possible for the polarization $\boldsymbol{\Xi}$ in the particle, provided that the extra stress $\boldsymbol{\tau}$ is also uniform in the particle. On the other hand, the constitutive equation (2.12) for the particle admits a uniform stress solution, $\boldsymbol{\tau}=\boldsymbol{\tau}^p$, provided that the strain rate and vorticity in the particle are uniform. Therefore, it is concluded that the solutions for the strain rate, $\boldsymbol{D}=\boldsymbol{D}^p$, and vorticity, $\boldsymbol{W}=\boldsymbol{W}^p$, are both uniform in the particle, and are determined in terms of the (uniform) particle polarization $\boldsymbol{\Xi}$ via

$$\boldsymbol{D}^p = \boldsymbol{D}^0 - \mathbb{P}\boldsymbol{\Xi}, \quad \boldsymbol{W}^p = \boldsymbol{W}^0 - \mathbb{R}\boldsymbol{\Xi}, \tag{3.16}$$

where $\mathbb{P}$ and $\mathbb{R}$ are constant, fourth-order, shape tensors, depending only on the particle geometry, and given by

$$\mathbb{P} = \frac{\det(\boldsymbol{Z})}{4\pi}\int_{|\boldsymbol{\xi}|=1} \mathbb{H}(\boldsymbol{\xi})|\boldsymbol{Z}\boldsymbol{\xi}|^{-3}\,\mathrm{d}S, \quad \mathbb{R} = \frac{\det(\boldsymbol{Z})}{4\pi}\int_{|\boldsymbol{\xi}|=1} \mathbb{T}(\boldsymbol{\xi})|\boldsymbol{Z}\boldsymbol{\xi}|^{-3}\,\mathrm{d}S. \tag{3.17}$$

It should be pointed out that the definition of the shape tensors here is different from the classical Eshelby tensors (Eshelby 1957 and 1959; Wetzel & Tucker 2001; see also Willis 1981 and Ponte Castañeda 2005 for more discussion on these choices).

Finally, it is noted that the uniform stress polarization $\boldsymbol{\Xi}$ and the uniform extra stress tensor in the particle, $\boldsymbol{\tau} = \boldsymbol{\tau}^p$, are related by

$$\boldsymbol{\Xi} = \boldsymbol{\tau}^p - 2\boldsymbol{D}^p. \tag{3.18}$$

Then, eliminating $\boldsymbol{\Xi}$ from (3.16), we obtain the following expressions for $\boldsymbol{D}^p$ and $\boldsymbol{W}^p$:

$$\boldsymbol{D}^p = (\mathbb{I} - 2\mathbb{P})^{-1}(\boldsymbol{D}^0 - \mathbb{P}\boldsymbol{\tau}^p), \tag{3.19}$$

$$\boldsymbol{W}^p = \boldsymbol{W}^0 - \mathbb{R}\boldsymbol{\tau}^p + 2\mathbb{R}[(\mathbb{I} - 2\mathbb{P})^{-1}(\boldsymbol{D}^0 - \mathbb{P}\boldsymbol{\tau}^p)], \tag{3.20}$$

where $\mathbb{I}$ is the fourth-order identity tensor (Willis 1981) and where $\boldsymbol{\tau}^p$ is determined by the differential equation

$$\frac{\mathrm{d}\boldsymbol{\tau}^p}{\mathrm{d}t} - (\boldsymbol{D}^p + \boldsymbol{W}^p)\boldsymbol{\tau}^p - \boldsymbol{\tau}^p(\boldsymbol{D}^p - \boldsymbol{W}^p) = \frac{2}{G}\boldsymbol{D}^p, \tag{3.21}$$

which has been obtained by setting the convective term equal to zero in the particle constitutive relation (2.12). It should be emphasized, in connection with expression (3.19), that the strain rate in the particle is such that $\mathrm{tr}\,\boldsymbol{D}^p = \boldsymbol{0}$, which is consistent with the incompressibility of the particle. In the next section, we will make use of this 'instantaneous' solution for an ellipsoidal elastic particle to construct time-dependent and steady-state solutions for the particle shape and orientation, as well as the stress, as functions of the applied loading conditions.

4. Particle deformation and rheological behaviour

In the previous section, we have seen that the instantaneous solution for the strain rate $\boldsymbol{D}^p$, vorticity $\boldsymbol{W}^p$ and extra stress $\boldsymbol{\tau}^p$ are all uniform inside an ellipsoidal elastic particle, and determined by relations (3.19), (3.20) and (3.21). On the other hand, it is a well-known fact that an ellipsoidal inclusion (regardless of its composition) subjected to a uniform strain rate and vorticity will deform through a series of ellipsoidal shapes – with evolving aspect ratios and orientation angles – as the applied deformation progresses. This means that the results (3.19), (3.20), as well as the constitutive equation (3.21), will continue to apply throughout the deformation history, except that the shape tensors $\mathbb{P}$ and $\mathbb{R}$ will change uniformly with the deformation, because of the evolution of the shape and orientation of the particle, as characterized by the tensor $\boldsymbol{Z}$. In the next subsections, we will make use of these observations to derive evolution equations for the response of an initially ellipsoidal particle to a general applied deformation, as defined by the prescribed tensors $\boldsymbol{D}^0$ and $\boldsymbol{W}^0$, as well as possible steady-state solutions for the particle deformation. Finally, we will obtain the macroscopic rheological properties of the suspension in the dilute limit.

4.1. *Evolution equations for the single particle deformation*

We begin by noting that the shape and orientation of the particles are completely determined by the aspect ratios and orientation of the axes of the ellipsoid. Recalling that a, b, c refer to the semi-axes of the ellipsoidal particles, we define the aspect ratios via $\omega_1 = b/a$ and $\omega_2 = c/a$, and let $\boldsymbol{n}_1$, $\boldsymbol{n}_2$, and $\boldsymbol{n}_3$ $(=\boldsymbol{n}_1 \times \boldsymbol{n}_2)$ be an orthonormal triad defining the directions of the principal axes of the ellipsoid. For simplicity, in this section, the Cartesian components of the stress and strain rate tensors will be referred to a fixed coordinate system (the principal coordinate) instantaneously coinciding with the triad $\boldsymbol{n}_1$, $\boldsymbol{n}_2$, and $\boldsymbol{n}_3$.

Then, by definition, the normal components of the strain rate in the principal coordinate are given by $D^p_{11} = (1/a)(\mathrm{d}a/\mathrm{d}t)$, $D^p_{22} = (1/b)(\mathrm{d}b/\mathrm{d}t)$ and $D^p_{33} = (1/c)(\mathrm{d}c/\mathrm{d}t)$, which leads to the following well-known (Bilby & Kolbuszewski 1977) evolution equations for the aspect ratios of the particle:

$$\left.\begin{aligned} \frac{\mathrm{d}\omega_1}{\mathrm{d}t} &= \omega_1(D^p_{22} - D^p_{11}), \\ \frac{\mathrm{d}\omega_2}{\mathrm{d}t} &= \omega_2(D^p_{33} - D^p_{11}). \end{aligned}\right\} \tag{4.1}$$

On the other hand, the evolution equations for the particle orientations can be written as (Bilby & Kolbuszewski 1977; Aravas & Ponte Castañeda 2004)

$$\frac{\mathrm{d}\boldsymbol{n}_i}{\mathrm{d}t} = \boldsymbol{\Omega}^p \boldsymbol{n}_i, \tag{4.2}$$

where $\boldsymbol{\Omega}^p$ is the (antisymmetric) spin tensor of the particle, which can be determined from well-known kinematic relations (Ogden 1984) and has components (in the principal coordinate)

$$\left.\begin{aligned} &\Omega^p_{12} = W^p_{12} - \frac{1+\omega_1^2}{1-\omega_1^2} D^p_{12}, \quad \Omega^p_{23} = W^p_{23} - \frac{\omega_1^2+\omega_2^2}{\omega_1^2-\omega_2^2} D^p_{23}, \\ &\Omega^p_{31} = W^p_{31} - \frac{\omega_2^2+1}{\omega_2^2-1} D^p_{13}. \end{aligned}\right\} \tag{4.3}$$

In addition, it is noted that the constitutive equation (3.21) may be rewritten as an evolution equation for the particle stress in the solid:

$$\frac{\mathrm{d}\boldsymbol{\tau}^p}{\mathrm{d}t} = (\boldsymbol{D}^p + \boldsymbol{W}^p)\boldsymbol{\tau}^p + \boldsymbol{\tau}^p(\boldsymbol{D}^p - \boldsymbol{W}^p) + \frac{2}{G}\boldsymbol{D}^p. \tag{4.4}$$

Finally, noting that the right-hand sides of equations (4.1), (4.2) with (4.3), and (4.4) depend on the components of $\boldsymbol{D}^p$ and $\boldsymbol{W}^p$, which in turn are known from (3.19) and (3.20) to depend on $\boldsymbol{\tau}^p$, as well as on ω_1, ω_2, $\boldsymbol{n}_1$, $\boldsymbol{n}_2$, and $\boldsymbol{n}_3$, it is concluded that equations (4.1), (4.2) and (4.4) provide a closed system of differential equations for the evolution of microstructural variables ω_1, ω_2, $\boldsymbol{n}_1$, $\boldsymbol{n}_2$, and $\boldsymbol{n}_3$, and the extra stress $\boldsymbol{\tau}^p$. More explicit forms for the evolution equations for both cylindrical and ellipsoidal particles subjected to a shear flow are given in Appendix A. It should also be pointed out that for given initial conditions, these equations can be easily integrated using a Runge–Kutta time-stepping scheme.

4.2. *Steady-state solutions for the single particle deformation*

As discussed earlier (see also § 5), steady-state solutions are expected under simple shear flow conditions at least for an initially circular two-dimensional particle. However, it should be emphasized that such steady-state solutions may only be achieved under special conditions, including the flow conditions, initial particle shape and material properties, and only the full integration of the evolution equations (4.1), (4.2) and (4.4), starting from some given initial conditions, can determine whether such steady-state solutions will be realized. But it is still important to characterize the conditions under which these steady-state solutions may exist.

In general, steady-state solutions may be determined by setting the right-hand sides of the evolution equations (4.1), (4.2) and (4.4) equal to zero, thus obtaining a set of 11 scalar equations in the 11 scalar unknowns provided by the six components of

the particle stress $\boldsymbol{\tau}^p$, the two aspect ratios, ω_1, ω_2, and the three orientational angles defined by the particle axes, $\boldsymbol{n}_1$, $\boldsymbol{n}_2$, and $\boldsymbol{n}_3$. However, certain simplifications of these equations are possible because of the special conditions that must be satisfied at a steady-state solution, which are worth detailing here.

First, the evolution equations for the aspect ratios (4.1), together with the incompressibility constraint in the particles $\mathrm{tr}\,\boldsymbol{D}^p = 0$, imply that, at steady state, the diagonal components of the particle strain rates in the principal coordinates of the particle must all vanish:

$$D^p_{11} = D^p_{22} = D^p_{33} = 0. \tag{4.5}$$

By means of expression (3.19) for the particle strain rate, these conditions provide two independent conditions on $\boldsymbol{\tau}^p$, ω_1, ω_2, $\boldsymbol{n}_1$, $\boldsymbol{n}_2$, and $\boldsymbol{n}_3$.

Next the evolution equations for the particle orientations, (4.2) with (4.3), imply that the particle strain rates and vorticity tensors must satisfy the three equations

$$W^p_{12} = \frac{1+\omega_1^2}{1-\omega_1^2} D^p_{12}, \quad W^p_{23} = \frac{\omega_1^2+\omega_2^2}{\omega_1^2-\omega_2^2} D^p_{23}, \quad W^p_{31} = \frac{\omega_2^2+1}{\omega_2^2-1} D^p_{13}, \tag{4.6}$$

which, together with expressions (3.19) and (3.20) for the particle strain rate and vorticity, provide three additional equations for the above-mentioned 11 unknowns.

Finally, using the fact, from (4.5), that the diagonal components of the particle strain rate tensor (relative to the particle axes) are zero, it can be easily shown from the normal components of expression (4.4) for the evolution of the extra particle stress tensor $\boldsymbol{\tau}^p$ that its shear components (again, relative to the particle axes) must all vanish:

$$\tau^p_{12} = \tau^p_{23} = \tau^p_{13} = 0. \tag{4.7}$$

Similarly, the three shear components of expression (4.4) for the evolution of the extra particle stress tensor $\boldsymbol{\tau}^p$ can be used to obtain three additional equations for the remaining eight unknowns:

$$(D^p_{ik} + W^p_{ik})\tau^p_{kj} + \tau^p_{ik}(D^p_{kj} - W^p_{kj}) + \frac{2}{G} D^p_{ij} = 0 \quad (i \neq j). \tag{4.8}$$

In conclusion, making use of (4.7) and (4.8) for the normal and shear components of the particle extra stress $\boldsymbol{\tau}^p$ in expressions (3.19) and (3.20) allows the determination of the particle strain rate $\boldsymbol{D}^p$ and vorticity $\boldsymbol{W}^p$ in terms of steady-state values of the aspect ratios, ω_1, ω_2, and the three orientational angles defined by the particle axes, $\boldsymbol{n}_1$, $\boldsymbol{n}_2$, and $\boldsymbol{n}_3$. Having thus eliminated the particle stresses, it follows that expressions (4.5) and (4.6) provide five independent equations for the two aspect ratios, ω_1 and ω_2, and the three orientational vectors, $\boldsymbol{n}_1$, $\boldsymbol{n}_2$, and $\boldsymbol{n}_3$.

In applications, however, (4.8) can become degenerate for certain special loading conditions, such as simple shear flow. For this reason, it is preferable to make direct use of the non-rate form of the particle constitutive relation (2.6). Thus, using the fact that, at steady state, the shear stresses are zero, it can be easily demonstrated that for initially spherical neo-Hookean (three-dimensional) particles

$$\left.\begin{aligned} G\tau^p_{11} &= (\omega_1\omega_2)^{-2/3} - 1, \quad G\tau^p_{22} = (\omega_1)^{4/3}(\omega_2)^{-2/3} - 1, \\ G\tau^p_{33} &= (\omega_2)^{4/3}(\omega_1)^{-2/3} - 1, \end{aligned}\right\} \tag{4.9}$$

while for initially circular (two-dimensional) particles

$$G\tau^p_{11} = \omega^{-1} - 1, \quad G\tau^p_{22} = \omega - 1. \tag{4.10}$$

Therefore, at steady state, the particle extra stress is completely determined in terms of the steady-state values of the particle aspect ratios. In §§ 5 and 6, (4.5) and (4.6) combined with (4.9) (or (4.10)) will be used to solve steady-state solutions for initially spherical (circular) particles.

4.3. *Macroscopic behaviour of a dilute suspension*

As already mentioned, in the dilute limit, the particles do not interact and the rheological behaviour of the suspension may be determined from the solution of the problem for the single particle in an infinite medium discussed in the previous subsections. Following Batchelor (1970) and Willis (1981), it is recalled that the average velocity gradient in the RVE – assumed to occupy a domain $\Omega = \Omega_p \bigcup \Omega_f$ (with subscripts p and f indicating the solid and fluid sections respectively) and to satisfy the affine boundary condition of the type (3.4) – is precisely $\boldsymbol{L}^0$. In other words, defining

$$\overline{\boldsymbol{L}} = \frac{1}{\mathrm{Vol}(\Omega)} \int_{\Omega} \boldsymbol{L}\, \mathrm{d}V, \tag{4.11}$$

and similarly for the average strain rate and vorticity tensors, $\overline{\boldsymbol{D}}$ and $\overline{\boldsymbol{W}}$, we have that $\overline{\boldsymbol{L}} = \boldsymbol{L}^0$, $\overline{\boldsymbol{D}} = \boldsymbol{D}^0$, and $\overline{\boldsymbol{W}} = \boldsymbol{W}^0$. It then follows that the average strain rate and vorticity in the particles is the same as for a single particle (since in the dilute limit all particles are the same), and we have, from (3.19) and (3.20), that

$$\boldsymbol{D}^p = (\mathbb{I} - 2\mathbb{P})^{-1}(\overline{\boldsymbol{D}} - \mathbb{P}\boldsymbol{\tau}^p), \tag{4.12}$$

$$\boldsymbol{W}^p = \overline{\boldsymbol{W}} - \mathbb{R}\boldsymbol{\tau}^p + 2\mathbb{R}[(\mathbb{I} - 2\mathbb{P})^{-1}(\overline{\boldsymbol{D}} - \mathbb{P}\boldsymbol{\tau}^p)], \tag{4.13}$$

which depend on the microstructural variables ω_1, ω_2, $\boldsymbol{n}_1$, $\boldsymbol{n}_2$, and $\boldsymbol{n}_3$, as well as on the stress $\boldsymbol{\tau}^p$ inside the particles, as determined by the evolution equations (4.1), (4.2) and (4.4).

On the other hand, the average stress $\bar{\boldsymbol{\sigma}}$ in the suspension may be expressed as

$$\bar{\boldsymbol{\sigma}} = \phi\, \bar{\boldsymbol{\sigma}}^p + (1 - \phi)\bar{\boldsymbol{\sigma}}^m, \tag{4.14}$$

where $\bar{\boldsymbol{\sigma}}^p = \boldsymbol{\sigma}^p = (1/\mathrm{Vol}(\Omega_p)) \int_{\Omega_p} \boldsymbol{\sigma}\, \mathrm{d}V$ is the average stress in the elastic particles, and $\bar{\boldsymbol{\sigma}}^m = (1/\mathrm{Vol}(\Omega_f)) \int_{\Omega_f} \boldsymbol{\sigma}\, \mathrm{d}V$ is the average stress in the surrounding fluid matrix, and $\phi = (\mathrm{Vol}(\Omega_p)/\mathrm{Vol}(\Omega)) \ll 1$ is the dilute volume fraction of the particles in the suspension. (Here, once again, we have made use of the fact that the average stress has the same uniform value in all the particles.) Now recalling that the pressure in both fluid and solid phases are indeterminate, expression (4.14) may be rewritten as

$$\bar{\boldsymbol{\sigma}} = -\bar{p}\, \boldsymbol{I} + \phi\, \boldsymbol{\tau}^p + (1 - \phi)\bar{\boldsymbol{\tau}}^m, \tag{4.15}$$

where $\bar{p}$ is the indeterminate mean pressure in the suspension, and $\boldsymbol{\tau}^p$ is the particle extra stress. Similarly, the average strain rate tensor can be expressed as

$$\overline{\boldsymbol{D}} = \phi\overline{\boldsymbol{D}}^p + (1 - \phi)\overline{\boldsymbol{D}}^m. \tag{4.16}$$

On the other hand, in the Newtonian fluid, the average stress $\bar{\boldsymbol{\tau}}^m$ is related to the average strain rate by

$$\bar{\boldsymbol{\tau}}^m = 2\overline{\boldsymbol{D}}^m, \tag{4.17}$$

(recall that we are working with dimensionless variables). Using (4.16) and (4.17), the average stress in the suspension, from (4.15), is given by

$$\bar{\boldsymbol{\sigma}} = -\bar{p}\boldsymbol{I} + 2\overline{\boldsymbol{D}} + \phi\, (\boldsymbol{\tau}^p - 2\boldsymbol{D}^p)\,. \tag{4.18}$$

Therefore, making use of the evolution equations (4.1), (4.2) and (4.4) to determine the extra stress $\boldsymbol{\tau}^p$ in the particle (together with the microstructural variables), and of expressions (4.12) and (4.13) for the strain rate $\boldsymbol{D}^p$ and vorticity $\boldsymbol{W}^p$ in the particle (in terms of $\boldsymbol{\tau}^p$ and the microstructural variables), we can see that expression (4.18) – together with appropriate initial conditions – serves to fully determine the average stress $\bar{\boldsymbol{\sigma}}$ in the dilute suspension, as a function of the (prescribed) average strain rate $\overline{\boldsymbol{D}}$ and vorticity tensor $\overline{\boldsymbol{W}}$. It should be emphasized that the constitutive model is both anisotropic (due to the evolving shape of the particles), as well as viscoelastic (due to the elasticity of the particles).

5. Idealized two-dimensional problem: circular particles in a simple shear flow

In this section, we consider the two-dimensional stress and deformation fields for a cylindrical particle with initially circular cross-section ($\omega_0 = 1$) and axis that is aligned with the x_3 direction, which is subjected to a simple shear flow (in the transverse plane) with $D^0_{12} = W^0_{12} = \dot{\gamma}/2$ (components relative to the fixed laboratory axes). In this case, there is only one aspect ratio $\omega = b/a$ and one orientation angle θ, so that the shape tensors $\mathbb{P}$ and $\mathbb{R}$ can be integrated analytically (see Appendix A), and the evolution equations for the particle aspect ratio ω, orientation θ, and particle stresses τ^p_{11}, τ^p_{22} and τ^p_{12} reduce to (A 8), and can be easily integrated numerically in time.

In addition to the results of the analytical theory described in the previous two sections, in this section, results obtained numerically with the ALE FEM solver of Gao & Hu (2009) are included for comparison purposes. For completeness, the details of the numerical simulation are described briefly in Appendix B. In general, at small Reynolds numbers, our two-dimensional numerical simulations suggest that the stress, strain rate and vorticity fields are uniform (though not constant) not only at steady state, but in fact throughout the entire deformation process, which is consistent with previous works of Roscoe (1967) and Goddard & Miller (1967). Figure 1 (see also Gao & Hu 2009 for more details) shows the initially circular particle after reaching a steady-state shape for a value of $G = 0.2$. In figure 1(*a*), the material elements on the particle boundary are seen to undergo a 'tank-treading' motion, analogous to the behaviour of vesicles (Keller & Skalak 1982). (Note that while the particle shape reaches a steady state, material points in the particle are undergoing a periodic motion.) In figure 1(*b*) (see also Gao & Hu 2009, for more details), the equilibrium shape can be seen to be fitted quite accurately by an ellipse, in agreement with the theoretical predictions and earlier work. As G increases, the elliptical shape becomes thread-like and more aligned with the mean flow direction, but the particle shape is still elliptic. Furthermore, the strain rate, the pressure and the extra stress field have all been found (not shown here) to be fairly uniform inside the particle, in agreement with the analytical solution for the fields in the elliptical particle.

In figure 2, the results of the analytical theory and the numerical simulations for the particle aspect ratio, orientation angle and extra stresses are presented for the case of $G = 0.2$. Both sets of results clearly show that the theoretical and numerical results for all the variables eventually reach steady-state values. More specifically, in figure 2(*a*), the transient solutions for the aspect ratio and orientation of the particle are also seen to compare quite well with the results obtained numerically with the ALE FEM solver of Gao & Hu (2009). There is a slight time delay in the FEM solutions due to the fact that in the numerical simulations (see Appendix B), the fluid phase is initially quiescent. After the channel walls are set to motion, it takes some time (about 0.15 dimensionless time units) for the shear flow to be developed in the domain.

The steady-state values for the particle shape, orientation, stresses and strain rates, may in fact be determined analytically from the solution of (4.5) and (4.6), together

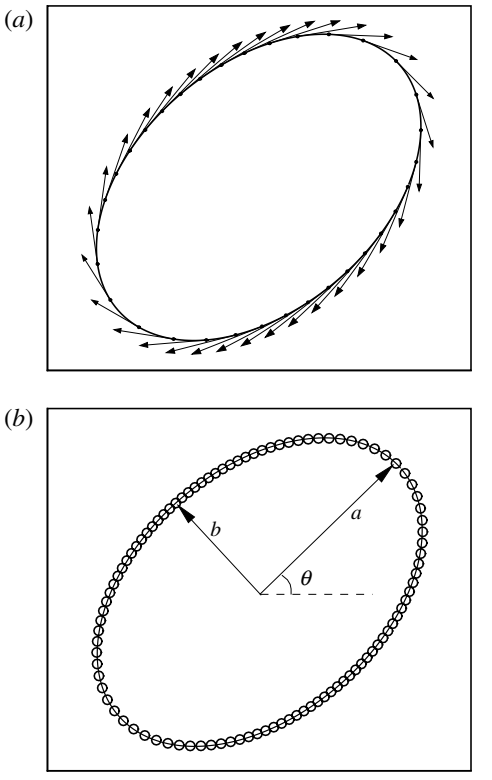

FIGURE 1. Particle deformation at $Re = 0.05$, $G = 0.2$ and $H = 10d_p$ at steady state. (*a*) 'Tank-treading' motion of material elements on particle boundary. (*b*) Equilibrium shape. The circles represent the computed result and the solid lines represent a standard ellipse: $(\bar{x}_1 \cos\theta + \bar{x}_2 \sin\theta)^2/a^2 + (-\bar{x}_1 \sin\theta + \bar{x}_2 \cos\theta)^2/b^2 = 1$.

with (4.10), and are given by

$$\omega = \frac{b}{a} = (\sqrt{1+G^2} - G)^2, \quad \theta = \frac{1}{2}\arctan\left(\frac{1}{G}\right), \tag{5.1}$$

$$\tau^p_{11} = 2(\sqrt{1+G^2} + G), \quad \tau^p_{22} = 2(G - \sqrt{1+G^2}), \tag{5.2}$$

$$D^p_{12} = G\sqrt{1+G^2}, \quad W^p_{12} = \frac{1}{2} + G^2, \tag{5.3}$$

$$\tau^p_{12} = D^p_{11} = D^p_{22} = 0, \tag{5.4}$$

where the components of the stress and strain rate are in the coordinates aligned with the principal axes of the particle. In figure 3, these steady-state results are also compared with the ALE FEM numerical results as functions of G, and excellent agreement is observed. (Note that the particle stress components are shown relative to the laboratory coordinates.) It is interesting to remark that the particle tends to stretch more and to become more aligned with the flow direction with increasing values of G (i.e. decreasing elastic stiffness of the particle). In addition, it can be seen that the normal stress component (τ^p_{11}) increases linearly with G, which is consistent with the increasing deformation of the particle. It should be noted, however, that in the limit as G tends to infinity, corresponding to a cavity in the fluid, the steady-state solution

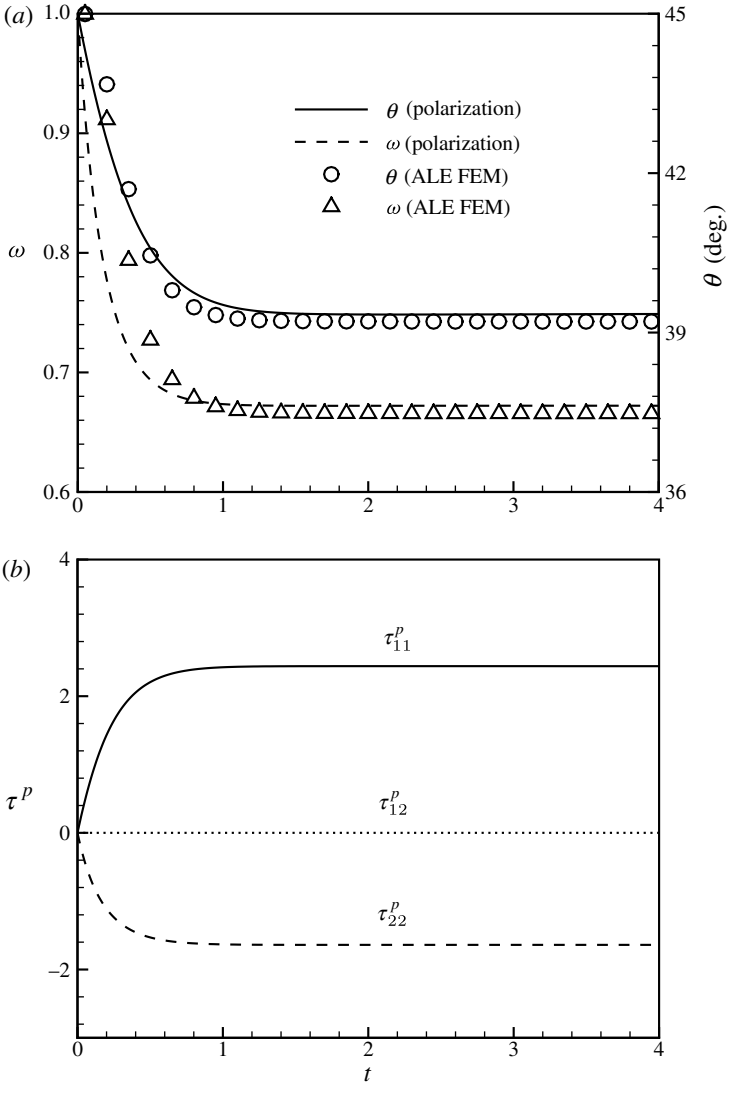

FIGURE 2. Analytical solutions (lines) for the two-dimensional time-dependent response at $G = 0.2$: (*a*) θ, ω, (*b*) τ_{11}^p, τ_{22}^p and τ_{12}^p (in the principal coordinates). Circles in (*a*) are the solutions obtained with ALE FEM.

is never reached, and the cavity continues to stretch and rotate indefinitely as the deformation proceeds.

To be able to describe the deformation in more quantitative terms, it is useful to introduce the deformation number

$$D = \frac{a-b}{a+b} = \frac{1-\omega}{1+\omega} = \frac{G}{\sqrt{1+G^2}}, \tag{5.5}$$

which is widely used in the measurement of deformation of droplets and vesicles (Stone 1994). It is noticed that for small deformation ($D < 0.2$), D linearizes as $G = D$. As G increases further, D gradually deviates from the straight line and the nonlinear behaviour becomes evident, as shown in figure 4.

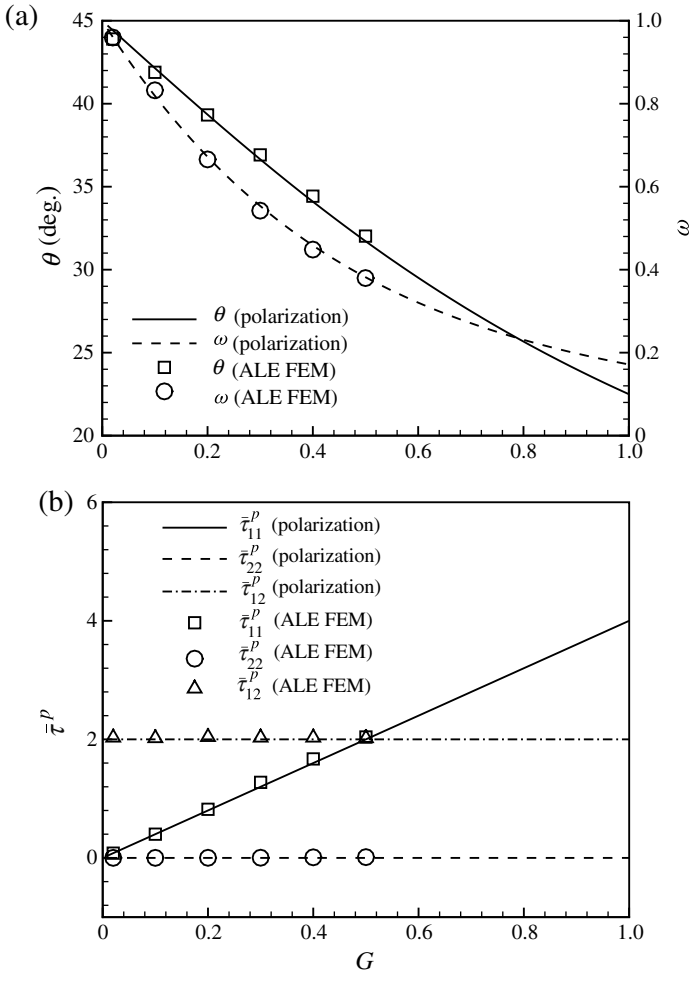

FIGURE 3. Comparisons of steady-state values from (5.1)–(5.4) with FEM results for a two-dimensional elastic particle, where lines are from (5.1)–(5.4) while the symbols are from FEM simulations. (*a*) Orientation angle θ and aspect ratio ω. (*b*) Components of the extra stress, $\boldsymbol{\tau}^p$, in laboratory coordinates. ($Re = 0.05$ in all FEM simulations.)

To assess the macroscopic response of the dilute dispersion of initially circular elastic particles, it is useful to introduce the effective viscosity of the dispersion, given by $\mu_{eff} = \bar{\sigma}_{12}/(2D^0_{12})$, as well as the corresponding (dimensionless) intrinsic viscosity

$$\mu'_{eff} = \frac{\mu_{eff} - 1}{\phi}, \tag{5.6}$$

which is independent of the particle volume fraction ϕ. It is also useful to define the dimensionless first and second normal stress differences (relative to the laboratory coordinates) via the expressions

$$\Pi_1 = \frac{\bar{\sigma}_{11} - \bar{\sigma}_{22}}{\phi}, \quad \Pi_2 = \frac{\bar{\sigma}_{22} - \bar{\sigma}_{33}}{\phi}, \tag{5.7}$$

which are also independent of concentration ϕ.

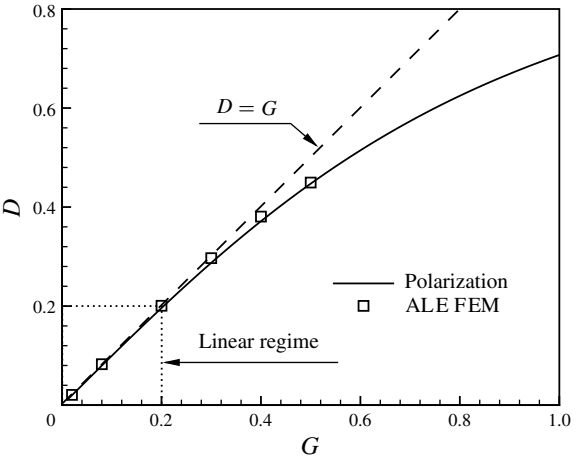

FIGURE 4. Deformation number D as a function of G. Solid line is from (5.5), symbols are computed data points from FEM simulation, and dash line is from the linear theory (Gao & Hu 2009).

For the dilute suspension of initially circular (two-dimensional) particles considered earlier in this section, it is easy to compute from the effective constitutive relation (4.18) the steady-state values of the intrinsic viscosity μ'_{eff} and the first normal stress difference Π_1 by using the solutions in (5.1)–(5.4) and rotating by an angle $-\theta$ back into the fixed laboratory coordinates. The result of this calculation is found to be

$$\mu'_{eff} = 2(1 - G^2), \quad \Pi_1 = 8G, \tag{5.8}$$

which, in full dimensional form (with superscript '$*$'), becomes

$$\mu^*_{eff} = \mu_f[1 + 2\phi(1 - G^2)], \quad \Pi^*_1 = 8\frac{\mu_f^2\dot{\gamma}^2\phi}{\eta_s} = \Psi_1\dot{\gamma}^2, \tag{5.9}$$

where $\Psi_1 = 8\phi\mu_f^2/\eta_s$ is called the coefficient of the first normal stress difference (Bird *et al.* 1987).

It can thus be deduced from (5.9) that for the two-dimensional particles the suspension undergoes shear thinning. Also, the two-dimensional Einstein viscosity $\mu^*_{eff} = \mu_f\,(1 + 2\phi)$ is recovered when $G \to 0$, corresponding to rigid inclusions. The particle deformation contributes to the effective viscosity only to second order in G, which is very similar to the rheological behaviour of a suspension of Newtonian droplets in another Newtonian liquid (Schowalter, Chaffey & Brenner 1968). It is interesting to notice that when $G > 1$, the intrinsic viscosity μ'_{eff} becomes negative, which means that the suspension has an effective viscosity that is less than that of the original fluid matrix. Also, the value $G = 1$ corresponds to a type of 'neutral' elastic particle which does not change the viscosity of the liquid. To understand this phenomenon, note that for $G = \mu_f\dot{\gamma}/\eta_s > 1$ the elastic force in the solid is less than the viscous force in the liquid, and thus the elastic particle becomes effectively more 'deformable' than the liquid outside, analogous to the situation of less viscous droplets in a more viscous matrix, as reported by Wetzel & Tucker (2001).

While it is clear that the intrinsic viscosity becomes negative for values of $G > 1$, care must be exercised to interpret the limit as $G \to \infty$, corresponding to a certain type of 'super-soft' particles, where the effective viscosity of the suspension may appear to tend to $-\infty$. However, in the limit of $G \to \infty$, both the aspect ratio and

the orientation angle from (5.1)–(5.4) tend to zero, indicating very slender particles. It was recognized by Batchelor (1971) that the dilute limit of the suspension of such thread-like soft particles requires $nl^3 \ll 1$ ($nl^2 \ll 1$ for two dimensions), where n is the fibre number density and l is fibre half-length. Using the analytical solutions derived above, it is thus easy to show that for a suspension of 'super-soft' neo-Hookean particles, the dilute limit requires $\phi \ll G^{-2}$, which guarantees the effective viscosity in (5.9) will remain positive – though less than that of the suspending fluid – in the domain of validity of the dilute estimate.

In an attempt to obtain a rough estimate for the domain of validity of the dilute expansion (5.8) for the effective behaviour of the suspension, we carried out a direct numerical simulation of a small amount of neo-Hookean particles in the shear flow by means of the monolithic ALE FEM solver (see Appendix B). The elastic particles are assumed to be identical and initially circular with diameter d_p. The effective stress field is calculated numerically according to formula (4.18). As shown in figure 5, the analytical results (5.8) for the dilute case agree very well with the numerical simulation for the smallest concentration ($\phi = 0.4\,\%$), but, as the concentration gradually increases ($\phi = 2, 4, 6, 8\,\%$), particle–particle interactions become progressively more important, and the dilute approximation ceases to be accurate. Thus, as a rule of thumb, we find that the dilute estimate should be quite accurate for concentrations less than about 1 %.

More specifically, figure 5(*a*) shows that the effective viscosity drops as G increases (or, equivalently, as the applied shear field becomes stronger). Thus, as already mentioned in the context of the dilute estimate, such a suspension of two-dimensional neo-Hookean particles undergoes shear thinning even at small but non-dilute concentrations. In addition, the effective viscosity grows more quickly with the concentration as the particles become stiffer. However, for very soft particles ($G \geqslant 0.3$), the effective viscosity becomes less sensitive to the variations in the concentration. Figure 5(*b*) shows that the first normal stress is always positive, meaning that the suspension tends to push the upper and bottom plates apart. It is also observed that, due to the larger deformation of the particles, the larger the value of G (the softer the particle), the higher the first normal stress difference in the suspension.

6. Initially spherical (three-dimensional) particle in a simple shear flow

In this section, a solution is provided for the three-dimensional problem of an elastic particle deforming in the simple shear flow ($D^0_{12} = W^0_{12} = \dot{\gamma}/2$) starting from an initially spherical shape. In this case, the evolution equations of § 4.1 specialize to (A 4) in Appendix A, which can be integrated numerically for the time-dependent solution. Typical results are shown in figure 6(*a–c*) for $G = 0.4$. Similar to the two-dimensional results in figure 2, in this case all the microstructural variables ω_1, ω_2, θ and the particle stress $\boldsymbol{\tau}^p$ also reach a steady state after transient deformation. In this context, it is interesting to observe, from figure 6(*b*), that the particle width in the transverse direction to the flow (*c*) increases slightly during the deformation, indicating that the three-dimensional flow field generated by the particle motion tends to stretch the particle in the z direction (neutral direction).

As discussed in § 4.2, the steady-state solutions can be obtained in two ways. First, we can solve the evolution equation (A 4) until it reaches steady state. Alternatively, the steady-state solutions can also be solved directly from (4.5)–(4.7) and (4.9). The results are shown (solid lines) in figure 7. Similar to the two-dimensional results, figures 7(*a*) and 7(*b*) show that the elastic particle also tends to stretch and align more with the flow direction with increasing G. In figure 7(*c*), a linear regime is observed for the deformation number D when $G < 0.2$, but with a different slope ($D \approx 1.24G$) than for the two-dimensional case.

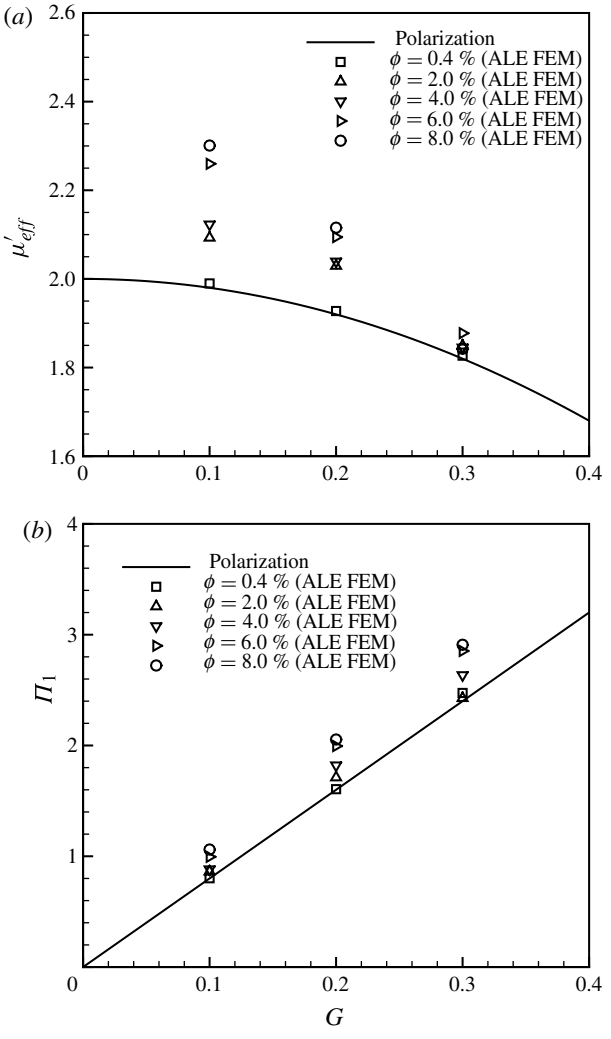

FIGURE 5. Rheological properties of the suspension (two dimensions): (*a*) intrinsic viscosity μ'_{eff}, (*b*) first normal stress difference Π_1.

Our three-dimensional steady-state results are also compared with the earlier results obtained by Roscoe (1967), using a different method, for the deformation of an initially spherical viscoelastic particle in a simple shear flow. In Roscoe's work, the shear stress component (τ^p_{12}) is assumed to be related to the shear component of the strain rate (D_{12}) by a constant 'material viscosity' η_1 (see (54) in Roscoe 1967). On the other hand, as we discussed in § 4.2, τ^p_{12} should be zero at steady state. To recover the solution for a pure elastic particle from Roscoe's work, it is necessary to take out the viscous contribution in the solid by setting the 'material viscosity' $\eta_1 = 0$. Excellent agreement is obtained with Roscoe's steady-state solution (shown in circles) for all the microstructural variables, as shown in figure 7(*a–c*), as well as the normal stress differences, as shown in figure 7(*d*).

In figure 8(*a*), the steady-state macroscopic rheological properties of a dilute suspension of three-dimensional elastic particles are shown as a function of G. It can be seen that the intrinsic viscosity μ'_{eff} decreases as G increases, indicating

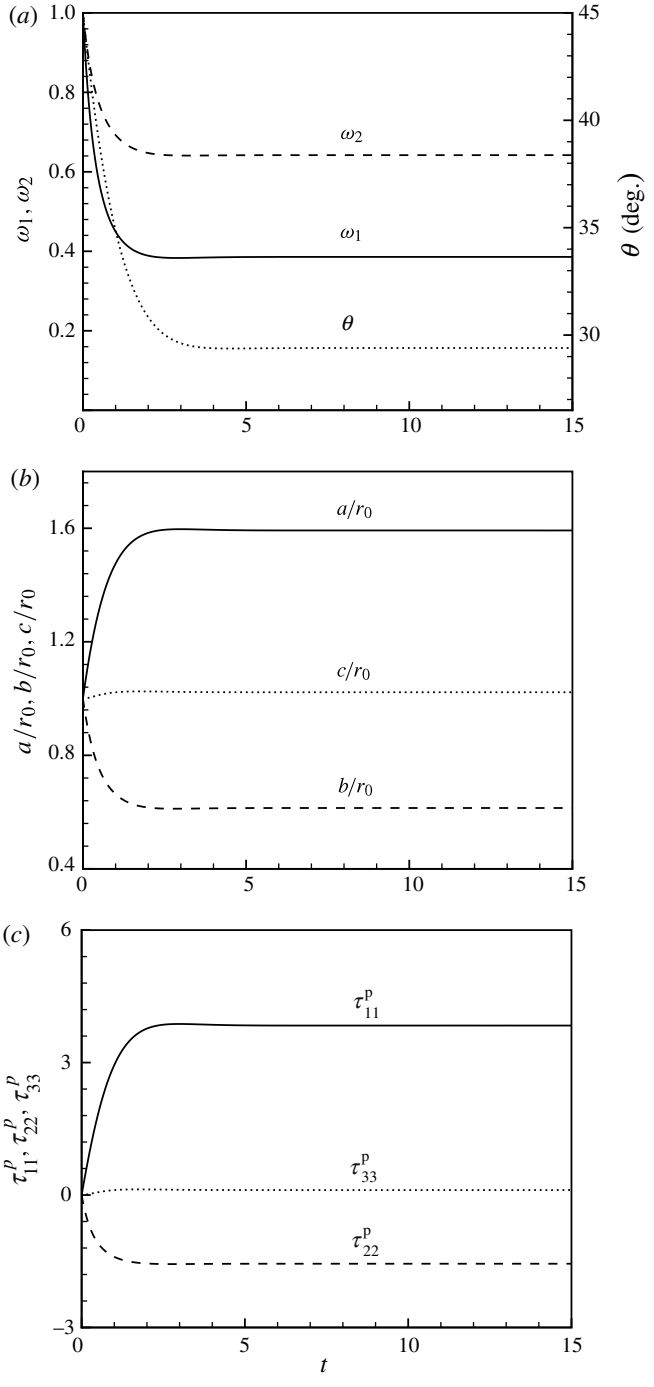

FIGURE 6. Time-dependent solutions for initially spherical (three-dimensional) particles at $G = 0.4$: (*a*) $\omega_1 = b/a$, $\omega_2 = c/a$, θ, (*b*) principal stretches a/r_0, b/r_0 and c/r_0, where r_0 is the initial radius of the sphere, (*c*) τ^p_{11}, τ^p_{22}, τ^p_{33} (in the principal coordinates). τ^p_{12} is found to be identically zero.

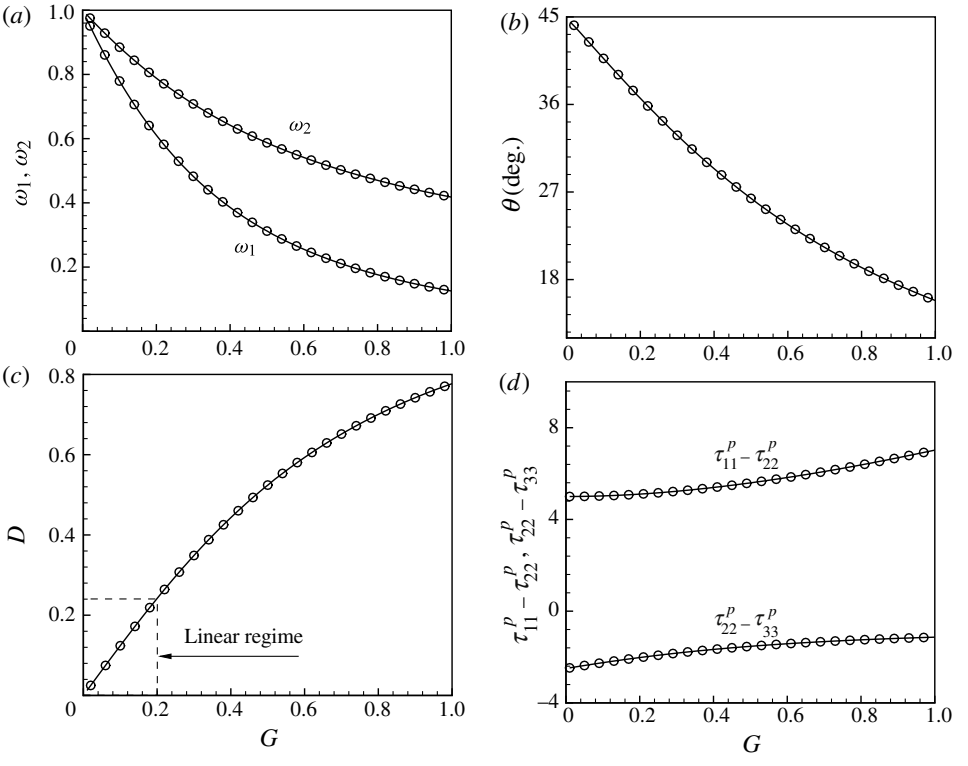

FIGURE 7. Steady-state particle deformation of an initially spherical sphere: (*a*) aspect ratio $\omega_1 = b/a$, $\omega_2 = c/a$, (*b*) orientation angle θ in the x–y plane, (*c*) deformation number $D = (1 - \omega_1)/(1 + \omega_1)$, (*d*) extra stress components τ^p_{11}, τ^p_{22} and τ^p_{33} (in the principal coordinates). The solid line represents the steady-state solution obtained from (4.5)–(4.7) and (4.9) The circles represent the equilibrium solution obtained by Roscoe (1967) with vanishing viscosity in the particle.

a shear-thinning behaviour. Also, when $G \to 0$, μ'_{eff} tends to the three-dimensional Einstein viscosity $\mu^*_{eff} = \mu_f\,(1 + 2.5\phi)$ for rigid particles. The critical value of G for 'neutral' particles where μ'_{eff} becomes negative is approximately 0.88, which is lower than that for the two-dimensional case. On the other hand, figure 8(*b*) shows that the effective first normal stress difference Π_1 is positive while the effective second normal stress difference Π_2 is negative. Both Π_1 and Π_2 grow monotonically with G, and the absolute value of Π_2 is roughly an order of magnitude smaller than Π_1, which is similar to the ratio commonly observed in polymeric fluids (Bird *et al.* 1987).

It should be emphasized that Roscoe's work was solely concerned with steady-state solutions. On the other hand, our work using the polarization technique can be used to obtain the full time evolution of rheological properties of the suspension directly from the time-dependent solutions for a single particle (figure 6), as shown in figure 9 for three typical G numbers, including the special case for 'neutral' particles ($G = 0.88$). Thus, figure 9(*a*) shows that the intrinsic viscosity μ'_{eff} exhibits an initial 'overshoot' and finally decays to the steady value. This overshoot is a consequence of the fact that the deformation and rotation of the elastic particle seem to take place over slightly

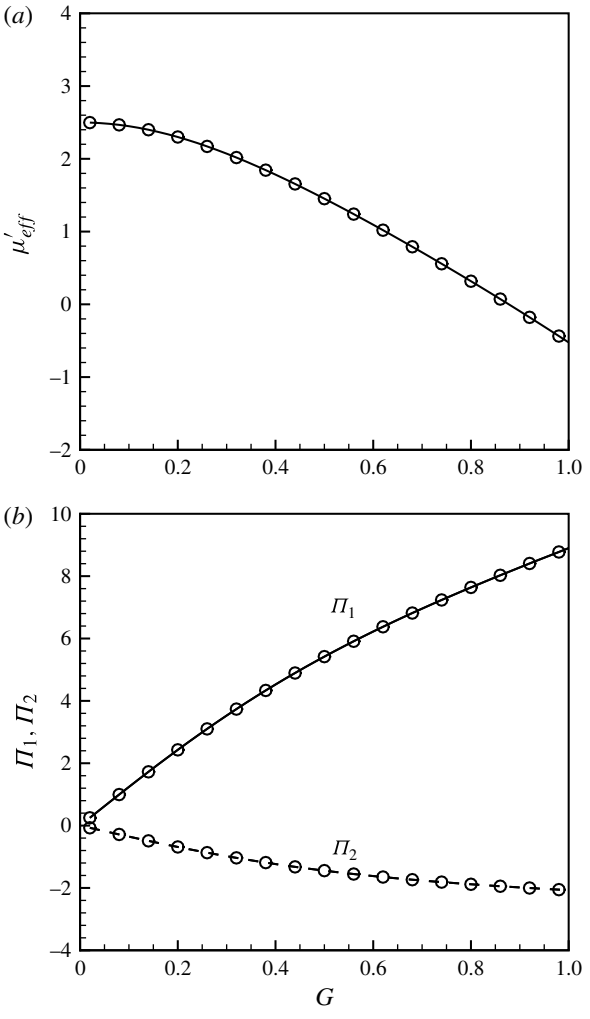

FIGURE 8. Steady-state rheological properties of the suspension (three dimensions): (*a*) intrinsic viscosity μ'_{eff}, (*b*) effective first (Π_1) and second (Π_2) normal stress differences. The lines represent the solution by our polarization technique, and the circles represent the solution by Roscoe's model (Roscoe 1967) without viscosity in solid.

different time intervals. As is evident from figure 6(*a*), the particle is both stretched and rotated as a consequence of the hydrodynamic loading. However, the particle keeps rotating after the stretching has been completed, continuing to become more and more aligned with the flow direction. This leads to a reduction in the viscosity μ'_{eff} and therefore to a lower plateau in the viscosity curves. Similar phenomena have also been observed for a Newtonian droplet in another Newtonian liquid (Wetzel & Tucker 2001).

7. Concluding remarks

By means of a polarization technique originally developed for the classical Eshelby problem in linear elasticity, a theory has been developed to describe the finite-strain,

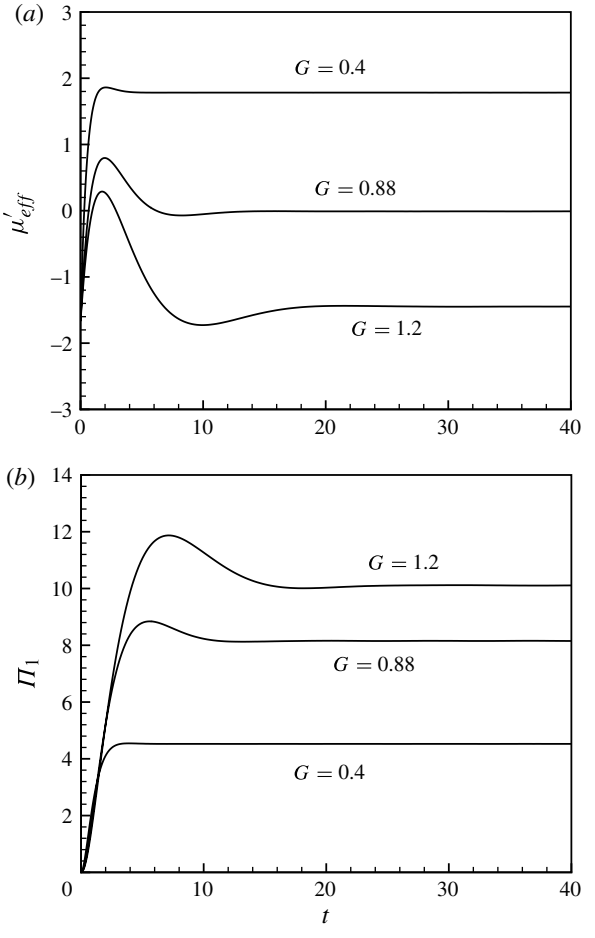

FIGURE 9. (*a*) Evolution of the three-dimensional intrinsic viscosity μ'_{eff} and (*b*) effective first normal stress difference Π_1.

time-dependent response of an ellipsoidal, neo-Hookean particle in a viscous fluid in the Stokes flow regime. The theory has been used to determine the deformation response of initially spherical (circular) particles in a simple shear flow, and in turn, the rheological behaviour of dilute suspensions of such particles.

In the numerical simulations of Gao & Hu (2009) for (two-dimensional) cylindrical particles, it was observed that an initially circular particle reaches a steady elliptical shape with all material elements undergoing a 'tank-treading' motion. Motivated by these observations, we have made use of the polarization technique to show rigorously that the velocity gradient and stress fields inside an elastic particle with an instantaneously ellipsoidal shape are uniform. This result implies that an elastic particle with an initially ellipsoidal shape will evolve through a sequence of ellipsoidal shapes, with possibly different aspect ratios and orientations. Using these results, a simple theory was developed for the evolution of the particle deformation and stresses in terms of a set of coupled, first-order, nonlinear ODEs. In addition, the theory was shown to admit steady-state solutions for initially circular (two-dimensional) and spherical (three-dimensional) particles under simple shear flow conditions. In particular, for initially circular particles in a shear flow, closed-form analytical solutions were

obtained, which were found to be in excellent agreement with the numerical solutions obtained using the ALE FEM of Gao & Hu (2009). For initially spherical particles, the steady-state solutions were obtained numerically. For both the two- and three-dimensional cases, the particle tends to become more stretched and aligned with the shear direction as the applied shear increases (G becomes larger). For the three-dimensional particle under shear flow, a three-dimensional flow field is generated around the particle, which tends to also stretch slightly the particle in the direction perpendicular to the flow, before reaching a steady-state value. We also compared successfully our three-dimensional steady-state solutions with those for a 'pure' elastic particle in the classical viscoelastic particle work of Roscoe (1967).

The effective properties of a dilute suspension of the elastic particles were determined from the single particle solution using standard results. Most interestingly, it has been found that elastic particles can reduce the effective viscosity of the suspension (relative to the viscosity of the suspending fluid) for sufficiently large values of G ($G > 1$ for two-dimensional particles and $G > 0.88$ for three-dimensional particles). This means that, depending on the shear flow rate, the elasticity of the particle can always be chosen such that a reduction in the viscosity of the fluid can be effected. This observation could turn out to be of practical value in applications. In addition, it was found that suspensions of both two- and three-dimensional elastic particles exhibit a shear-thinning effect in general. For the two-dimensional case, closed-form analytical expressions were obtained for the effective viscosity and the first normal stress difference. The results were compared with the corresponding results from a two-dimensional numerical simulation of multiple particles in a shear flow using the ALE FEM solver. When the concentration is small ($\phi < 1\,\%$), the FEM results for the effective viscosity and normal stress difference were found to be in excellent agreement with the two-dimensional analytical solutions. However, as the concentration is increased beyond this level, particle–particle interactions become important and the FEM results start to deviate from the dilute solutions. In three dimensions, the time evolution of the rheological properties of the suspension was also investigated. An initial overshoot in the effective viscosity was observed due to different time scales for the particle deformation and rotation to reach their steady-state values. However, the effective viscosity eventually settles into its equilibrium value as the deformed particle rotates into the flow direction.

Finally, it is worthwhile emphasizing that the new theory is able to capture the time evolution of all relevant physical variables in the elastic particle. The resulting set of coupled, first-order, nonlinear ODEs can be easily integrated numerically for given initial conditions. Although, in this paper, we have restricted our attention to initially spherical (circular) particles in a shear flow, it is straightforward to apply the theory for other cases. For example, Jeffery's solution (Jeffery 1922) involving a periodic tumbling motion for a rigid ellipsoidal particle in the shear flow can be easily recovered by letting $G \to 0$. The solution for a cavity with an ellipsoidal shape, which yields increasingly elongated shapes that become more and more aligned with the flow direction, never quite reaching a steady state, can also be easily derived by letting $G \to \infty$. The case of an initially ellipsoidal particle with finite elasticity leads to a rich class of behaviours which will be investigated in some detail in a future publication. It should also be emphasized that this theory can be applied to more general flow conditions (e.g. pure strain, angular deformation, etc.), as long as the velocity gradient of the external flow field is uniform, and the particle concentration of the suspension is small enough. Under these conditions, the solution procedure outlined in this paper provides a systematic and efficient way to describe the particle dynamics and rheological properties of the suspension.

The work of T.G. and H.H.H. was partially supported by the Nano/Bio Interface Center at the University of Pennsylvania through the NSF NSEC DMR-045780. The work of P.P.C. was supported by the National Science Foundation under NSF grant number CMMI-0969570.

Appendix A. Particle deformation in a shear flow

Here we present the solution procedure for particle deformation in a simple shear flow. During the particle deformation, we assume the particle rotates in the $\bar{x}_1$–$\bar{x}_2$ plane with the angular velocity $\mathrm{d}\theta/\mathrm{d}t$ and also undergoes a homogeneous deformation. Following Roscoe (1967), the unperturbed shear field in the laboratory coordinates $\bar{\boldsymbol{u}}^0 = (\bar{x}_2, 0, 0)$ can be transformed into the principal coordinate $\{x_i\}$, which is instantaneously aligned with axes of the particle

$$\left.\begin{aligned} u_1^0 &= \tfrac{1}{2}\sin(2\theta)x_1 + \cos^2(\theta)x_2, \\ u_2^0 &= -\sin^2(\theta)x_1 - \tfrac{1}{2}\sin(2\theta)x_2, \\ u_3^0 &= 0. \end{aligned}\right\} \tag{A 1}$$

Therefore, the non-zero components of the strain rate ($\boldsymbol{D}^0$) and the vorticity tensor ($\boldsymbol{W}^0$) are given by

$$D_{11}^0 = \tfrac{1}{2}\sin(2\theta), \quad D_{22}^0 = -\tfrac{1}{2}\sin(2\theta), \quad D_{12}^0 = \tfrac{1}{2}\cos(2\theta), \quad W_{12}^0 = \tfrac{1}{2}. \tag{A 2}$$

In general, the fourth-order tensors $\mathbb{P}$ and $\mathbb{R}$ can be written in 'contracted' notation, relative to the principal coordinates, as (Kailasam & Ponte Castañeda 1998)

$$\left.\begin{aligned} \mathbb{P}_{mn} &= \begin{bmatrix} \mathbb{P}_{11} & \mathbb{P}_{12} & \mathbb{P}_{13} & 0 & 0 & 0 \\ \mathbb{P}_{12} & \mathbb{P}_{22} & \mathbb{P}_{23} & 0 & 0 & 0 \\ \mathbb{P}_{13} & \mathbb{P}_{23} & \mathbb{P}_{33} & 0 & 0 & 0 \\ 0 & 0 & 0 & \mathbb{P}_{44} & 0 & 0 \\ 0 & 0 & 0 & 0 & \mathbb{P}_{55} & 0 \\ 0 & 0 & 0 & 0 & 0 & \mathbb{P}_{66} \end{bmatrix}, \\ \mathbb{R}_{mn} &= \begin{bmatrix} 0 & 0 & 0 & 0 & 0 & 0 \\ 0 & 0 & 0 & 0 & 0 & 0 \\ 0 & 0 & 0 & 0 & 0 & 0 \\ 0 & 0 & 0 & \mathbb{R}_{44} & 0 & 0 \\ 0 & 0 & 0 & 0 & \mathbb{R}_{55} & 0 \\ 0 & 0 & 0 & 0 & 0 & \mathbb{R}_{66} \end{bmatrix}. \end{aligned}\right\} \tag{A 3}$$

Details of the contracted notation for fourth-order tensors can be found in Wetzel & Tucker (2001). As an example, $\mathbb{R}_{66} = \mathbb{R}_{1212} = \mathbb{R}_{1221} = -\mathbb{R}_{2112}$. For our case, $\mathbb{P}_{44} = \mathbb{P}_{55} = \mathbb{R}_{44} = \mathbb{R}_{55} = 0$. Then, (3.19), (3.20) can be used to solve for $\boldsymbol{D}^p$ and $\boldsymbol{W}^p$.

The time-dependent ODEs given by (4.1), (4.3) and (4.4) reduce to

$$\left.\begin{aligned}
\frac{\mathrm{d}\tau_{11}^p}{\mathrm{d}t} &= 2D_{11}^p\tau_{11}^p + 2(D_{12}^p + W_{12}^p)\tau_{12}^p + \frac{2}{G}D_{11}^p,\\
\frac{\mathrm{d}\tau_{22}^p}{\mathrm{d}t} &= 2D_{22}^p\tau_{22}^p + 2(D_{12}^p - W_{12}^p)\tau_{12}^p + \frac{2}{G}D_{22}^p,\\
\frac{\mathrm{d}\tau_{33}^p}{\mathrm{d}t} &= 2D_{33}^p\tau_{33}^p + \frac{2}{G}D_{33}^p,\\
\frac{\mathrm{d}\tau_{12}^p}{\mathrm{d}t} &= (D_{12}^p + W_{12}^p)\tau_{22}^p + (D_{12}^p - W_{12}^p)\tau_{11}^p - D_{33}^p\tau_{12}^p + \frac{2}{G}D_{12}^p,\\
\frac{\mathrm{d}\omega_1}{\mathrm{d}t} &= \omega_1(D_{22}^p - D_{11}^p),\\
\frac{\mathrm{d}\omega_2}{\mathrm{d}t} &= \omega_2(D_{33}^p - D_{11}^p),\\
\frac{\mathrm{d}\theta}{\mathrm{d}t} &= \left(\frac{1+\omega_1^2}{1-\omega_1^2}\right)D_{12}^p - W_{12}^p,
\end{aligned}\right\} \tag{A 4}$$

where $\tau_{13}^p = \tau_{23}^p = 0$.

For two-dimensional particles, $\mathbb{P}$ and $\mathbb{R}$ take the form

$$\mathbb{P} = \frac{\det(\boldsymbol{Z})}{2\pi}\int_{|\boldsymbol{\xi}|=1}\mathbb{H}\,(\xi_1,\xi_2,\xi_3=0)\,|\boldsymbol{Z}\boldsymbol{\xi}|^{-2}\mathrm{d}S, \tag{A 5}$$

$$\mathbb{R} = \frac{\det(\boldsymbol{Z})}{2\pi}\int_{|\boldsymbol{\xi}|=1}\mathbb{T}\,(\xi_1,\xi_2,\xi_3=0)\,|\boldsymbol{Z}\boldsymbol{\xi}|^{-2}\mathrm{d}S, \tag{A 6}$$

with the two-dimensional shape tensor $\boldsymbol{Z} = \mathrm{diag}\{a, b\}$. The non-zero components of these two tensors can be computed analytically and are given by

$$\mathbb{P}_{11} = \mathbb{P}_{22} = -\mathbb{P}_{12} = \frac{\omega}{2(\omega+1)^2}, \quad \mathbb{P}_{66} = \frac{\omega^2+1}{4(\omega+1)^2} \quad \text{and} \quad \mathbb{R}_{66} = -\frac{\omega-1}{4\,(\omega+1)}. \tag{A 7}$$

In this two-dimensional case, the unknowns are τ_{11}^p, τ_{22}^p, τ_{12}^p, θ and $\omega = b/a$, and the required equations reduce to

$$\left.\begin{aligned}
\frac{\mathrm{d}\tau_{11}^p}{\mathrm{d}t} &= 2D_{11}^p\tau_{11}^p + 2(D_{12}^p + W_{12}^p)\tau_{12}^p + \frac{2}{G}D_{11}^p,\\
\frac{\mathrm{d}\tau_{22}^p}{\mathrm{d}t} &= 2D_{22}^p\tau_{22}^p + 2(D_{12}^p - W_{12}^p)\tau_{12}^p + \frac{2}{G}D_{22}^p,\\
\frac{\mathrm{d}\tau_{12}^p}{\mathrm{d}t} &= (D_{12}^p + W_{12}^p)\tau_{22}^p + (D_{12}^p - W_{12}^p)\tau_{11}^p + \frac{2}{G}D_{12}^p,\\
\frac{\mathrm{d}\omega}{\mathrm{d}t} &= -2\omega D_{11}^p,\\
\frac{\mathrm{d}\theta}{\mathrm{d}t} &= \left(\frac{1+\omega^2}{1-\omega^2}\right)D_{12}^p - W_{12}^p.
\end{aligned}\right\} \tag{A 8}$$

It should be emphasized that all the equations above are given in the fixed coordinate system which instantaneously coincides with the particle axes. However, it is difficult to integrate the stress equations, since the time derivative of these stress variables, for example $\mathrm{d}\tau_{11}/\mathrm{d}t$, is usually approximated by the difference between the values $\tau_{11}^{(n+1)}$ at the time step t_{n+1} and $\tau_{11}^{(n)}$ at the current time step t_n. One has to keep

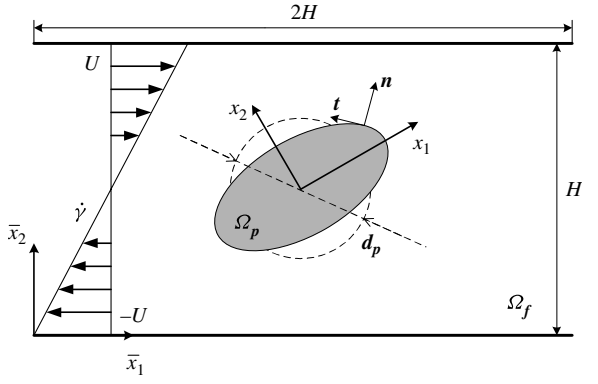

FIGURE 10. Schematic for elastic particles deforming in the shear flow bounded by moving walls.

in mind that in this case $\tau_{11}^{(n+1)}$ is still defined in the current fixed principal coordinates at t_n. Thus, after each time step, $\tau_{11}^{(n+1)}$ has to be transformed again into a new principal coordinate at t_{n+1}. To avoid this difficulty, one can transform the evolution equations of these stress components into a rotating principal coordinate system which is always aligned with the particle axes. Here we define $\boldsymbol{n}_1, \boldsymbol{n}_2, \boldsymbol{n}_3$ to be the three unit vectors for these rotating principal coordinates. Thus the extra solid stress tensor is written as

$$\boldsymbol{\tau}^p = \tau_{11}^p \boldsymbol{n}_1\boldsymbol{n}_1 + \tau_{22}^p \boldsymbol{n}_2\boldsymbol{n}_2 + \tau_{33}^p \boldsymbol{n}_3\boldsymbol{n}_3 + \tau_{12}^p(\boldsymbol{n}_1\boldsymbol{n}_2 + \boldsymbol{n}_2\boldsymbol{n}_1), \tag{A 9}$$

where the components τ_{13}^p and τ_{23}^p are zero. Notice that the time derivative of the unit vectors are given by $\mathrm{d}\boldsymbol{n}_1/\mathrm{d}t = (\mathrm{d}\theta/\mathrm{d}t)\boldsymbol{n}_2$, $\mathrm{d}\boldsymbol{n}_2/\mathrm{d}t = -(\mathrm{d}\theta/\mathrm{d}t)\boldsymbol{n}_1$, $\mathrm{d}\boldsymbol{n}_3/\mathrm{d}t = 0$. It is easy to verify that the time derivatives of the stress components in the rotating coordinates (represented with an overdot) and in the fixed coordinates are related by

$$\dot{\tau}_{11}^p = \frac{\mathrm{d}\tau_{11}^p}{\mathrm{d}t} + 2\tau_{12}^p\frac{\mathrm{d}\theta}{\mathrm{d}t}, \quad \dot{\tau}_{22}^p = \frac{\mathrm{d}\tau_{22}^p}{\mathrm{d}t} - 2\tau_{12}^p\frac{\mathrm{d}\theta}{\mathrm{d}t}, \tag{A 10}$$

$$\dot{\tau}_{33}^p = \frac{\mathrm{d}\tau_{33}^p}{\mathrm{d}t}, \quad \dot{\tau}_{12}^p = \frac{\mathrm{d}\tau_{12}^p}{\mathrm{d}t} - (\tau_{11}^p - \tau_{22}^p)\frac{\mathrm{d}\theta}{\mathrm{d}t}, \tag{A 11}$$

which are valid for both the two- and three-dimensional cases. After the transformation, an appropriate time-stepping method, such as the Runge–Kutta scheme, can then be applied directly.

Appendix B. Numerical simulation for the two-dimensional case

To solve the idealized two-dimensional problem, we consider an initially circular elastic particle of diameter d_p that is neutrally buoyant in a shear flow confined between two parallel plates, as shown in figure 10. The computational size of the domain is chosen as $2H \times H$. Here, we use $\{x_i\}$ to denote the principal coordinates which instantaneously coincide with the semi-axes of the ellipse, and $\{\bar{x}_i\}$ for the (fixed) laboratory coordinates. In the $\bar{x}_1$–$\bar{x}_2$ plane, a simple shear field $\dot{\gamma} = 2U/H$ is generated by sliding the upper and bottom walls in the opposite directions with a constant velocity U. In addition, periodic boundary conditions are used at the two ends in the $\bar{x}_1$ direction.

The monolithic ALE solver with a mixed finite element (Gao & Hu 2009) is briefly described next. In general, different interpolation functions are chosen for different

unknown variables, specifically, the fluid velocity is approximated by piecewise quadratic functions which are continuous all over the domain (P2), while the pressure is piecewise linear (P1) and the stress components are piecewise quadratic (P2) (Hu *et al.* 2001). For this study, the temporal discretization implemented in the solver is a second-order finite difference scheme. Numerical simulations were carried out with channel separations at $H = 5d_p, 8d_p, 10d_p, 20d_p$ respectively, to confirm that the wall effect on the particle deformation is negligible. It was found that the differences between computed results of θ and ω are less than 1 % when $H > 5d_p$. Therefore, we use $H = 10d_p$ in all simulations in the paper.

REFERENCES

ARAVAS, N. & PONTE CASTAÑEDA, P. 2004 Numerical methods for porous metals with deformation-induced anisotropy. *Comput. Meth. Appl. Mech. Engng* **193**, 3767–3805.

BARNES, H. A. 1994 Rheology of emulsions: a review. *Colloids Surf.* A **91**, 89–95.

BARTHÈS-BIESEL, D. 1980 Motion of a spherical microcapsule freely suspended in a linear shear flow. *J. Fluid Mech.* **100**, 831–853.

BARTHÈS-BIESEL, D. & RALLISON, J. M. 1981 The time-dependent deformation of a capsule freely suspended in a linear shear flow. *J. Fluid Mech.* **113**, 251–267.

BATCHELOR, G. K. 1970 The stress system in a suspension of force-free particles. *J. Fluid Mech.* **41**, 545–570.

BATCHELOR, G. K. 1971 The stress generated in a non-dilute suspension of elongated particles by pure straining motion. *J. Fluid Mech.* **46**, 813–829.

BILBY, B. A., ESHELBY, J. D. & KUNDU, A. K. 1975 The change of shape of a viscous ellipsoidal region embedded in a slowly deforming matrix having a different viscosity. *Tectonophysics* **28**, 265–274.

BILBY, B. A. & KOLBUSZEWSKI, M. L. 1977 The finite deformation of an inhomogeneity in two-dimensional slow viscous incompressible flow. *Proc. R. Soc. Lond.* A **355**, 335–353.

BIRD, R. B., ARMSTRONG, R. C., HASSAGER, O. & CURTISS, C. F. 1987 *Dynamics of Polymeric Liquids, Kinetic Theory,* vol. 2. Wiley.

CERF, R. 1952 On the frequency dependence of the viscosity of high polymer solutions. *J. Chem. Phys.* **20**, 395–402.

CHIEN, S., USAMI, S., DELLENBACK, R. J. & GREGERSEN, M. I. 1967*a* Blood viscosity: influence of erythrocyte aggregation. *Science* **157**, 829–831.

CHIEN, S., USAMI, S., DELLENBACK, R. J. & GREGERSEN, M. I. 1967*b* Blood viscosity: influence of erythrocyte deformation. *Science* **157**, 827–829.

EINSTEIN, A. 1906 Eine neue Bestimmung der Molekül-dimensionen. *Ann. Phys.* **324**, 289–306. Corrections, ibid, 339, 591–592.

ESHELBY, J. D. 1957 The determination of the elastic eld of an ellipsoidal inclusion, and related problems. *Proc. R. Soc. Lond.* A **241**, 376–396.

ESHELBY, J. D. 1959 The elastic eld outside an ellipsoidal inclusion. *Proc. R. Soc. Lond.* A **252**, 561–569.

FRÖHLICH, H. & SACK, R. 1946 Theory of the rheological properties of dispersions. *Proc. R. Soc. Lond.* A **185**, 415–430.

GAO, T. & HU, H. H. 2009 Deformation of elastic particles in viscous shear flow. *J. Comput. Phys.* **228**, 2132–2151.

GEL'FAND, I. M. & SHILOV, G. E. 1964 *Generalized Functions, vol. 1: Properties and Operations*. Academic.

GHIGLIOTTI, G., BIBEN, T. & MISBAH, C. 2010 Rheology of a dilute two-dimensional suspension of vesicles. *J. Fluid Mech.* **653**, 489–518.

GODDARD, J. D. & MILLER, C. 1967 Nonlinear effects in a rheology of dilute suspensions. *J. Fluid Mech.* **28**, 657–673.

HIRT, C. W., AMSDEN, A. A. & COOK, J. L. 1974 An arbitrary Lagrangian–Eulerian computing method for all flow speeds. *J. Comput. Phys.* **14**, 227–253.

HU, H. H., ZHU, M. Y. & PATANKAR, N. 2001 Direct numerical simulations of fluid–solid systems using the arbitrary Lagrangian–Eulerian technique. *J. Comput. Phys.* **169**, 427–462.

JEFFERY, G. B. 1922 The motion of ellipsoidal particles immersed in a viscous fluid. *Proc. R. Soc. Lond.* A **102**, 161–179.

JOSEPH, D. D. 1990 *Fluid Dynamics of Viscoelastic Liquids*, *Applied Mathematical Sciences*, vol. 84. Springer.

KAILASAM, M. & PONTE CASTAÑEDA, P. 1998 A general constitutive theory for linear and nonlinear particulate media with microstructure evolution. *J. Mech. Phys. Solids* **46**, 427–465.

KELLER, S. R. & SKALAK, R. 1982 Motion of a tank-treading ellipsoidal particle in a shear flow. *J. Fluid Mech.* **120**, 27–47.

LAC, E., BARTHÈS-BIESEL, D., PELEKASIS, N. A. & TSAMOPOULOS, J. 2004 Spherical capsules in three-dimensional unbounded Stokes flows: effect of the membrane constitutive law and onset of buckling. *J. Fluid Mech.* **516**, 303–334.

LE TALLEC, P. & MOURO, J. 2001 Fluid structure interaction with large structural displacements. *Comput. Meth. Appl. Mech. Engng* **190**, 3039–3067.

MACOSKO, C. W. 1994 *Rheology: Principles, Measurements and Applications*. VCH.

MASUD, A. & HUGHES, T. J. R. 1997 A space–time Galerkin/least-squares finite element formulation of the Navier–Stokes equations for moving domain problems. *Comput. Meth. Appl. Mech. Engng* **146**, 91–126.

MATTSSON, J., WYSS, H. M., FERNANDEZ-NIEVES, A., MIYAZAKI, K., HU, Z., REICHMAN, D. R. & WEITZ, D. A. 2009 Soft colloids make strong glasses. *Nature* **462**, 83–86.

MURATA, T. 1981 Deformation of an elastic particle suspended in an arbitrary flow field. *J. Phys. Soc. Japan* **50**, 1009–1016.

OGDEN, R. W. 1984 *Nonlinear Elastic Deformations*. Dover.

OLDROYD, J. G. 1953 The elastic and viscous properties of emulsions and suspensions. *Proc. R. Soc. Lond.* A **218**, 122–132.

PONTE CASTAÑEDA, P. 2005 *Heterogeneous materials*. *Lecture Notes*, Department of Mechanics, Ecole Polytechnique.

PONTE CASTAÑEDA, P. & WILLIS, J. R. 1995 The effect of spatial distribution on the effective behaviour of composite materials and cracked media. *J. Mech. Phys. Solids* **43**, 1919–1951.

RAMANUJAN, S. & POZRIKIDIS, C. 1998 Deformation of liquid capsules enclosed by elastic membranes in simple shear flow: large deformations and the effect of capsule viscosity. *J. Fluid Mech.* **361**, 117–143.

RIVLIN, R. S. 1948 Large elastic deformation of isotropic materials. I. fundamental concepts. *Phil. Trans. R. Soc.* A **240**, 459–490.

ROSCOE, R. 1967 On the rheology of a suspension of viscoelastic spheres in a viscous liquid. *J. Fluid Mech.* **28**, 273–293.

RUMSCHEIDT, F. D. & MASON, S. G. 1961 Particle motions in sheared suspensions. Part XII. Deformation and burst of fluid drops in shear and hyperbolic flow. *J. Colloid Sci.* **16**, 238–261.

SCHOWALTER, W. R., CHAFFEY, C. E. & BRENNER, H. 1968 Rheological behaviour of a dilute emulsion. *J. Colloid Interface Sci.* **26**, 152–160.

SNABRE, P. & MILLS, P. 1999 Rheology of concentrated suspensions of viscoelastic particles. *Colloids Surf. A Physicochem Engng Asp.* **152**, 79–88.

STONE, H. A. 1994 Dynamics of drop deformation and breakup in viscous flows. *Annu. Rev. Fluid Mech.* **26**, 65–102.

SUBRAMANIAM, A. B., ABKARIAN, M., MAHADEVAN, L. & STONE, H. A. 2005 Non-spherical gas bubbles. *Nature* **438**, 930.

TAYLOR, G. I. 1934 The formation of emulsions in definable fields of flow. *Proc. Roy. Soc. Lond.* A **146**, 501–523.

WETZEL, E. D. & TUCKER, C. L. 2001 Droplet deformation in dispersions with unequal viscosities and zero interfacial tension. *J. Fluid Mech.* **426**, 199–228.

WILLIS, J. R. 1981 Variational and related methods for the overall properties of composites. *Adv. Appl. Mech.* **21**, 1–78.